INVESTIGATION OF THE EFFECT OF OIL GROOVE IN THE PERFORMANCE OF A COMPRESSOR PISTON

A THESIS SUBMITTED TO
THE GRADUATE SCHOOL OF NATURAL AND APPLIED SCIENCES
OF
MIDDLE EAST TECHNICAL UNIVERSITY

BY

BİLGİN HACIOĞLU

IN PARTIAL FULFILLMENT OF THE REQUIREMENTS
FOR
THE DEGREE OF MASTER OF SCIENCE
IN
MECHANICAL ENGINEERING

DECEMBER 2006

Approval of the Graduate School of Natural and Applied Sciences

Prof. Dr. Canan Özgen
Director

I certify that this thesis satisfies all the requirements as a thesis for the degree of Master of Science.

Prof. Dr. S. Kemal İder
Head of the Department

This is to certify that we have read this thesis and that in our opinion it is fully adequate, in scope and quality, as a thesis for the degree of Master of Science.

Prof. Dr. Zafer Dursunkaya
Supervisor

Examining Committee Members

Prof. Dr. Faruk Arınç	(METU, ME)	_____
Prof. Dr. Zafer Dursunkaya	(METU, ME)	_____
Assoc. Prof. Dr. Serkan Özgen	(METU, AE)	_____
Instr. Dr. Yiğit Yazıcıoğlu	(METU, ME)	_____
Dr. Hüsnü Kerpiççi	(ARÇELİK A.Ş)	_____

I hereby declare that all information in this document has been obtained and presented in accordance with academic rules and ethical conduct. I also declare that, as required by these rules and conduct, I have fully cited and referenced all material and results that are not original to this work.

Name, Last name: Bilgin Hacıoğlu

Signature :

ABSTRACT

INVESTIGATION OF THE EFFECT OF OIL GROOVE
IN THE PERFORMANCE OF A COMPRESSOR PISTON

Hacıoğlu, Bilgin
M.S., Mechanical Engineering Department
Supervisor: Prof. Dr. Zafer Dursunkaya

December 2006, 81 pages

Oil feed grooves are implemented in reciprocating compressor piston applications to assure a constant supply of lubricating oil on bearing surfaces and decrease friction loss. In a hermetically sealed compressor, due to small clearances encountered, oil supply becomes critical in order not to operate in boundary lubrication regime. Due to the small size of the piston and small piston – cylinder clearance, a partial lubrication regime is present. In the current study, a model that solves Reynolds' equation for piston-cylinder lubrication and the average Reynolds' equation that considers the effect of roughness on partially lubricated bearing for a compressor piston with oil feed grooves is developed. A parametric study is carried out to investigate the effects of piston design parameters and then arrive at an improved piston performance by using alternative designs for oil feed groove and the other design parameters.

Keywords: Hydrodynamic lubrication, boundary lubrication, reciprocating hermetic compressor, piston-cylinder lubrication, oil groove

ÖZ

YAĞ KANALININ KOMPRESOR PİSTONUNUN PERFORMANSI ÜZERİNDEKİ ETKİSİNİN İNCELENMESİ

Hacıoğlu, Bilgin
Yüksek Lisans, Makine Mühendiliği Bölümü
Tez Yöneticisi: Prof. Dr. Zafer Dursunkaya

Aralık 2006, 81 sayfa

Gitmeli gelmeli kompresör pistonlarında, yağ kanalı pistona yağın ulaşmasını sağlamak ve sürtünme kayıplarını azaltımak için uygulanmaktadır. Hermetik kompresörlerde piston silindir eşleşmesi küçük boşluklarla yapıldığından pistonun sınır yağlama şartlarında çalışmaması için, yağın piston yeterli yatağında bulunması önem kazanmakadır. Bu çalışma ile piston-slindir yatağındaki yağlamayı tanımlayan Reynolds denklemi ve sınır yağlama şartlarınıda yüzey prüzlülüğü etkisini içeren ortalama Reynolds denklemini çözen bir model geliştirilmiştir. Yapılan parametrik çalışma sonucunda tasarım değişkenlerinin etkisi araştırılmış ve piston performansını arttıran alternatif piston yağ kanalı tasarımına ulaşılmıştır.

Anahtar kelimeler: Hidrodinamik yağlama, sınır yağlama, gitmeli gelmeli hermetik kompresör, piston-silindir yağlaması, yağ kanalı

To My Family

ACKNOWLEDGMENTS

The author would like to express his deep gratitude to his supervisor Prof. Dr. Zafer Dursunkaya, who made this work happen, for his guidance, supervision and encouragement.

The author also wishes to thank to his family, friends and all members of Arçelik Compressor Plant Product Development Department for their support and encouragement.

TABLE OF CONTENTS

LIST OF TABLES

TABLES

LIST OF FIGURES

FIGURES

NOMENCLATURE

A : Coefficient matrix of pressures
a_4 : Piston axial acceleration
B : Coefficient matrix of film thicknesses
B_p : Length of inclined pad bearing
c : Radial clearance
C_p : Center of percussion
E : Composite elastic modulus
e : Eccentricity of the piston center of mass from cylinder axis
F_{gas} : Gas force on piston
F_{34} : Force on wristpin
F_1 : Known boundary pressure matrix
F_{gas} : Gas force on piston head
F_{x34} : Side force between piston and cylinder
F_z : Axial force on piston
f : Friction coefficient
G_3 : Connecting rod center of mass
H : Nondimensional clearance profile of the inclined pad
I_G : Piston mass moment of inertia at its center of mass
J : Jacobian matrix
$\tilde{h}$: Film thickness array
h_1 : Inclined pad film thickness at inlet
h_0 : Inclined pad film thickness at outlet
h_T : Local film thickness
h : Nominal film thickness
h^{old} : Film thickness in previous time step
h_{dyn} : Clearance due to geometry
h_{grv} : Clearance due to groove
h_m : Crank eccentricity
Hr : Hardness
k : Wear coefficient
L : Bearing axial length
L_p : Inclined pad bearing width
l : Connecting rod length
l_A : Distance from center of mass to big end of connecting rod
l_B : Distance from center of mass to small end of connecting rod
l_P : Distance from center of percussion to center of mass of connecting rod
m_3 : Connecting rod mass
m_{3b} : Connecting rod mass concentrated at wristpin
m_{3p} : Connecting rod mass concentrated at center of percussion
m_3 : Piston mass
P : Hydrodynamic oil pressure
P_c : Boundary contact pressure

P_{gas} : Cylinder gas pressure
P_{sc} : Suction pressure
$\widetilde{P}_u$: Unknown internal grid pressure array
R : Piston radius
s : Cylinder axis-crank center misalignment
t : Time
T : Compressor time period
U, U_z : Sliding velocity of the piston
W : Wear load
z : Piston axial position
$\dot{z}$: Piston axial speed
α : Crank angle
α_{tilt} : Piston tilt angle
β : Connecting rod angle
$\dot{\beta}$: Connecting rod angular speed
$\ddot{\beta}$: Connecting rod angular acceleration
ε : Piston skirt eccentricity
$\ddot{\varepsilon}$: Piston skirt eccentricity acceleration
ϕ_z, ϕ_θ : Pressure flow factors
ϕ_s : Shear flow factor
ϕ_{fs}, ϕ_{fp} : Shear stress factors
μ : Viscosity of the lubricant
γ : Elipticity ratio
θ : Angular coordinate on the piston
$\bar{\tau}$: Mean shear flow
η : Asperity density
ζ : Radius of curvature of asperity tops
σ : Asperity heights
ω : Crank rotational speed
ϖ : Wear rate in volume per distance
τ : Shear stress
IP_{hyd} : Hydrodynamic power loss
IP_{bdy} : Friction (boundary) power loss

CHAPTER I

1. INTRODUCTION

In reciprocating compressor piston applications piston cylinder clearance value is kept small primarily to prevent leak back of the refrigerant through piston-cylinder clearance. However, the clearance value becomes critical from lubrication point of view, as the piston starts working in mixed or boundary lubrication regime. Because of the asperity contacts, oil flow is prevented, causing a drop in oil film pressure and decrease in load carrying capacity of the bearing.

Application of circumferential oil feed groove is very common in reciprocating compressor pistons. The lubrication issue of the groove is to provide oil supply to the bearing surfaces, and also to reduce power loses by reducing the bearing-sliding area. The design problem of the groove is reducing the power lose due to piston friction while assuring the reliability of the piston and minimizing the leak back of the refrigerant.

The lateral motions of the piston during piston sliding motion inside a cylinder are named secondary dynamics. The simulation of piston secondary motion requires the solution of equations of motion of the piston in axial and lateral directions simultaneously. The sliding motion in axial direction is determined by analyzing the slider crank mechanism, and the equations of motion in lateral direction are solved coupled with the lubrication equation known as Reynolds' equation.

Reynolds' equation is a second order elliptical partial differential equation and is solved using a rigid piston-cylinder assumption. The equations of motion in lateral direction are solved using the calculated oil film hydrodynamic pressure, boundary contact pressure, gas pressure and inertia forces determined form slider crank dynamics and lubrication analyze.

A parametric study is carried with the developed software to reach an optimum oil feed groove design with a cooperative solutions of Reynolds' equation with average Reynolds' equation, which describes the effect of small clearances on lubrication dynamics.

1.1 Aim of the Study

Increasing efficiency demands in domestic refrigeration industry enforces compressor manufacturers to design lower energy consuming compressors by decreasing the thermodynamic, flow, electrical and friction losses of the compressors they produce. An ongoing compressor design project, called MTS, is carried at Arçelik Compressor Plant by Research and Development Department. One of the major goals of the project is to significantly reduce the friction loses of the new model with respect to existing compressor models. Bearing researches are done for a few years in the company and there is significant knowledge accumulation about journal bearings, however piston-cylinder bearing has not been studied in detail.

With this study a numerical code is developed to solve the lubrication dynamics of the piston-cylinder bearing. Hence after analyzing and understanding the physics of the piston lubrication, an optimum piston design is suggested for the new MTS compressor by decreasing the friction loses with an optimum bearing design from lubrication and reliability point of view.

1.2 Hermetic Reciprocating Compressor

In domestic refrigeration applications vapor-compression refrigeration cycle is used which is the most preferred refrigeration type. A simple vapor-compression refrigeration cycle is shown in figure 1.1. The refrigerant enters the compressor as a slightly superheated vapor at a low pressure. It then leaves the compressor and

enters the condenser as a vapor at some elevated pressure, where the refrigerant is condensed as a result of heat transfer to the lower temperature surroundings. The refrigerant then leaves the condenser as a high-pressure liquid. The pressure of the liquid is decreased as it flows through the expansion valve and, as a result, some of the liquid flashes into vapor. The remaining liquid, now at a low pressure, is vaporized in the evaporator as a result of heat transfer from the refrigerated space. This vapor than enters the compressor.

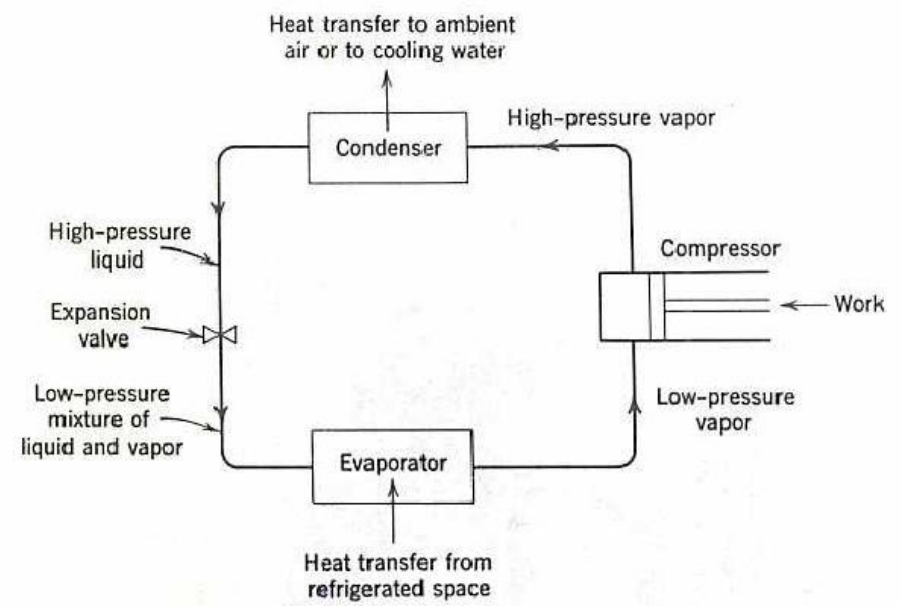

Figure 1.1 Schematic diagram of a simple refrigeration cycle

For compressors used in domestic refrigerators reciprocating compressors, dominated the market for several years, because of the high reliability of the their slider crank mechanism, relatively low acoustic noise level and comparative lower costs.

Reciprocating compressors are available in various designs; the difference among them is related to the way the reciprocating motion of the piston is generated. Traditionally, the motion of the piston to compress the refrigerant gas has been generated by the use of a scotch-yoke or slider-crank mechanism, converting a rotating motion into an oscillating motion.

1.3 Lubrication

When opposing bearing surfaces are completely separated by a lubricant film, fluid film lubrication occurs. The pressure generated within the fluid by the various mechanisms carries load applied on the bearings. The study related to the mechanisms, which prevent surfaces from damage during sliding by implementing a lubricant between them, is called lubrication.

The primary studies of the basis of the theory of lubrication began with the experimental studies of B. Tower [1] emphasizing for the first time the existence of hydrodynamic pressure in the lubricant film of a bearing. And Petrov [2] reached the same conclusion from friction measurements. However the modern hydrodynamic lubrication theory is established by Osborne Reynolds in 1886 by publishing a celebrated analytical paper [3] in which he used a reduced form the Navier-Stokes equations in association with the continuity equation to explain Tower's experimental results and give physical explanation of the load carrying capacity due to the conversion of the rate of flow in the oil wedge.

Reynolds hydrodynamic description was found to break down for very thin films that for order of ten molecular diameters. The boundary lubrication term is first introduced by Hardy and Doubleday [4,5] to describe the condition, in which lubricant film that is reduced in thickness. They found that molecular properties, such as molecular weight and molecular arrangement are governing the frictional force in extremely thin films adhering to surfaces that are often sufficient to assist relative sliding. They concluded that under such circumstances the chemical composition of the lubricant is important since the physical and chemical properties of thin films of molecular proportions and the surfaces to which they are attached determine the contact behavior. The concept was greatly extended by the work of Bowden and Tabor [6] who investigated friction form the perspective of elastic process.

In recent years researches has been carried on to understand the other lubrication regimes such as elasto-hydrodynamic lubrication that pressures are relatively high and elastic deformation of surfaces occurs and the viscosity of the lubricant rises. Also on “partial lubrication” or “mixed lubrication”, which is a combined mode between boundary lubrication and hydrodynamic lubrication.

In hydrodynamic bearings pressure and fluid film generations sufficient to separate surfaces rely only on the geometry and relative motion of the sliding surfaces together with the viscous nature of the fluid. The fluid film generated is thick enough to completely separate the surfaces, and the pressure developed is not large enough to cause elastic deformations. Because of the relative motion of the surfaces and the viscosity of the lubricant, positive pressure occurs, which carries the normal load and separates the surfaces. Two motion characteristics shown in figure 1.2; sliding, where the lubricant film thickness must be decreasing in sliding direction, wedge effect; and squeeze action where bearing surfaces approach each other with a certain squeezing velocity, generate pressure.

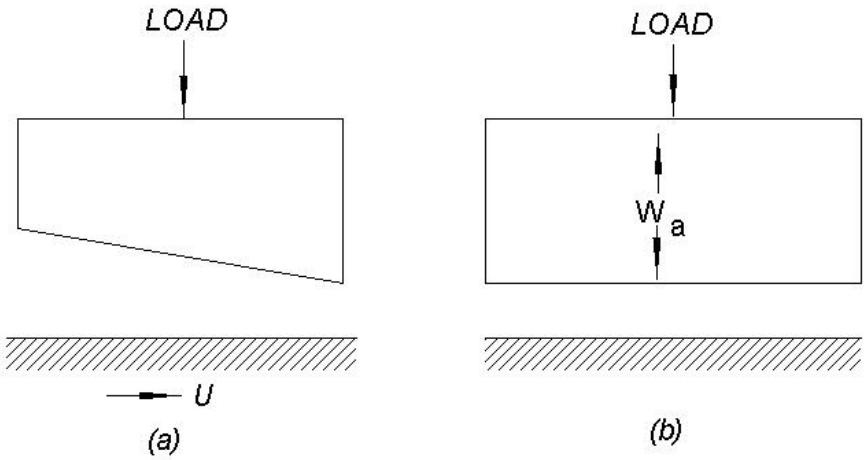

Figure 1.2 Pressure development mechanisms for hydrodynamic lubrication. (a) Slider bearing (wedge effect) with velocity U; (b) squeeze film bearing with squeezing velocity W_a

In hydrodynamic lubrication in some applications pressure of the fluid film is large enough to cause elastic deformation on the bearing surfaces. Under

conditions of extreme pressure the behavior of the conventional mineral lubricating oils can be non-Newtonian. The type of lubrication considering these effects is called elasto-hydrodynamic lubrication, in which the presence of deformations causes variations in pressure and film thickness profiles of the bearings.

When the specific load is very high, or the relative sliding speed is not high enough, it is difficult to build up sufficiently thick film to entirely separate the bearing faces, and so there will be some mechanical interaction between opposing surface asperities. This is inevitable, even allowing for the large increase in effective lubricant viscosity and the elastic flattening of the surface profile that can occur in the elasto-hydrodynamic regime. Eventually the highest regions of the surfaces may be protected by lubricant films literally only a few molecules thick and it is this state of affairs that is known as boundary lubrication.

In partial lubrication or mixed lubrication regime some contacts take place between asperities. The combined mechanism of fluid film lubrication and boundary lubrication is present and one or more molecular layers of the boundary lubricating films are in interaction with each other.

Detailed explanation of lubrication history and lubrication regimes are in Hamrok [7], Frene et. al. [8] and Williams [9].

1.3.1 Lubrication of a Piston

One of the bearings that must be designed for reliability and performance in a reciprocating compressor is the piston of the slider crank mechanism a model of which is shown in figure 1.3. The piston does a reciprocating motion inside a cylinder hole. With the linear motion of the piston, the refrigerant gas is first sucked into the cylinder, then compressed and finally exhaled out of the cylinder.

The solid model of the piston-cylinder is shown in figure 1.3. The piston has a circumferential oil groove. There are holes on the groove opening inside the piston that is opened to compressor inside. Hence pressure around the groove is equal to compressor suction pressure. Skirt side of the piston is opened inside the compressor shell and the head side is opened inside the cylinder hole and does work on the refrigerant gas. As a result at the piston head boundary, pressure is equal to cylinder hole pressure that is the refrigerant gas pressure.

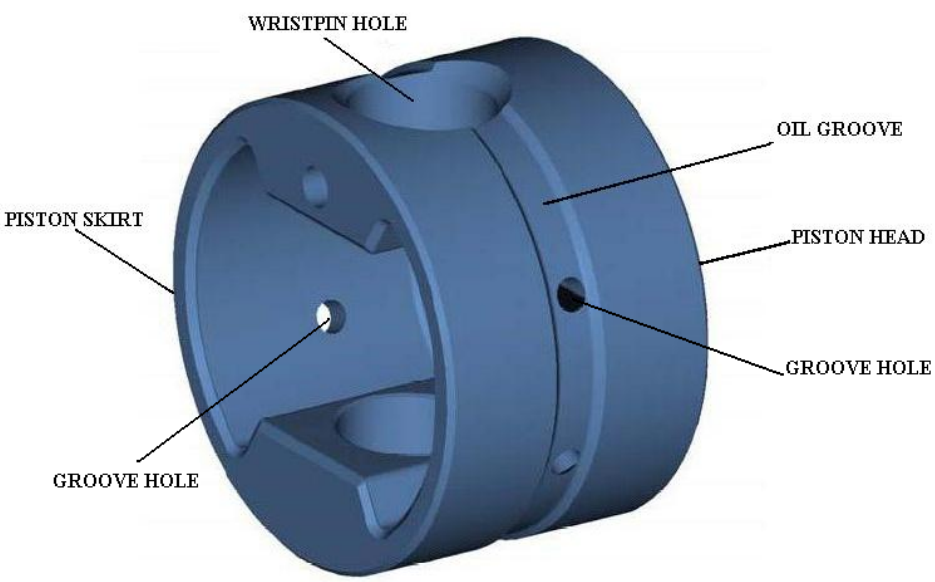

Figure 1.3 Solid model of a compressor piston

The design problem of the piston of a compressor is to minimize the boundary contact and wear so that to increase the life and decrease the power loss, meanwhile to prevent the leak back of the refrigerant gas through the clearances of sliding lubricated surfaces. There is a certain clearance value between the piston and cylinder walls that is determined by the designer. An oil groove is preferred on the piston-bearing surface; primarily to decrease the sliding area of the piston so that to reduce the friction loses.

In figure 1.4 a view of the slider crank mechanism of a reciprocating compressor is shown. There is a pin assembly slot is machined vertically across cylinder hole in order to be able to assemble the wristpin through piston wristpin and connecting rod small end holes. This slot affects lubrication since it decreases the lubricated area.

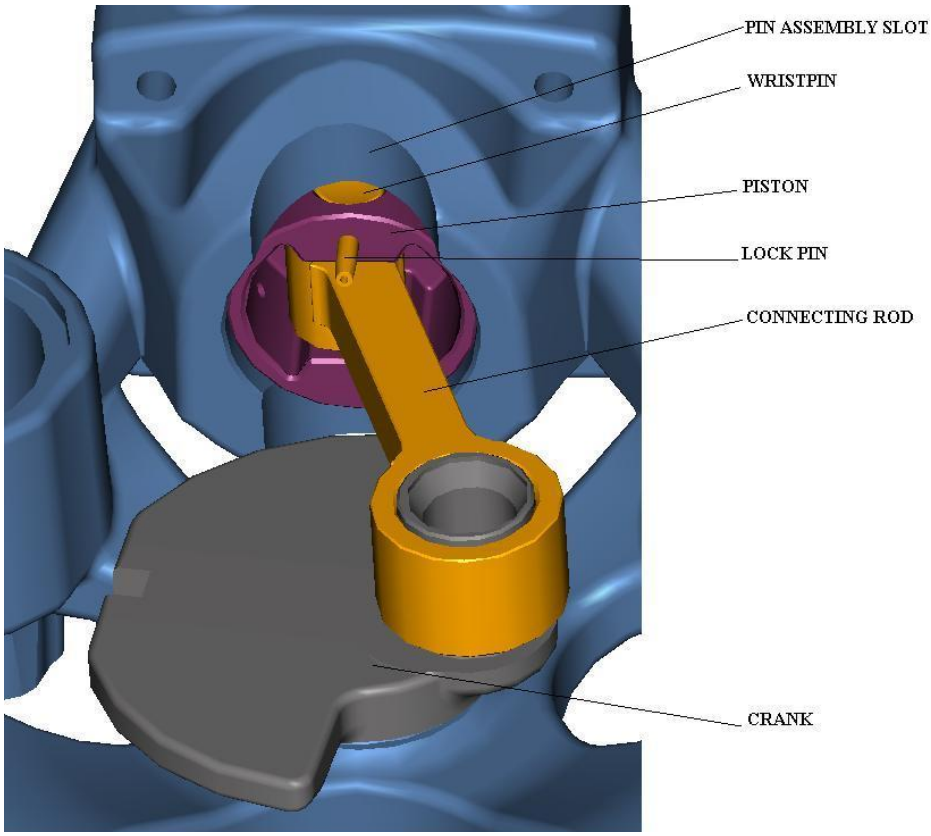

Figure 1.4 Model of the slider-crank assembly of a reciprocating compressor

In the field of lubrication phenomenon of a reciprocating piston there are many studies carried out in recent years especially for automotive applications. Goenka and Meernik [10] describe the analysis methods developed for piston lubrication analysis and comparing the friction prediction of each of these methods with data obtained from an experimental rig designed to measure piston-assembly friction. The results are presented to demonstrate the effect of some design parameters on the lubrication performance of a piston skirt. Figure 1.5 illustrated one of the

results they obtained for the effect of piston mass on friction for two different pin offsets.

Keribar and Dursunkaya [11] solve hydrodynamic lubrication problem and present a general model for the solution of secondary motion analysis of conventional and articulated piston assemblies. Axial, lateral and rotational departures in positions and motions from kinematics, resulting from clearances within the piston assembly components and cylinder are solved. Figure 1.6 shows the effect of load on skirt tilt, and the skirt lateral motion of the skirt top and bottom.

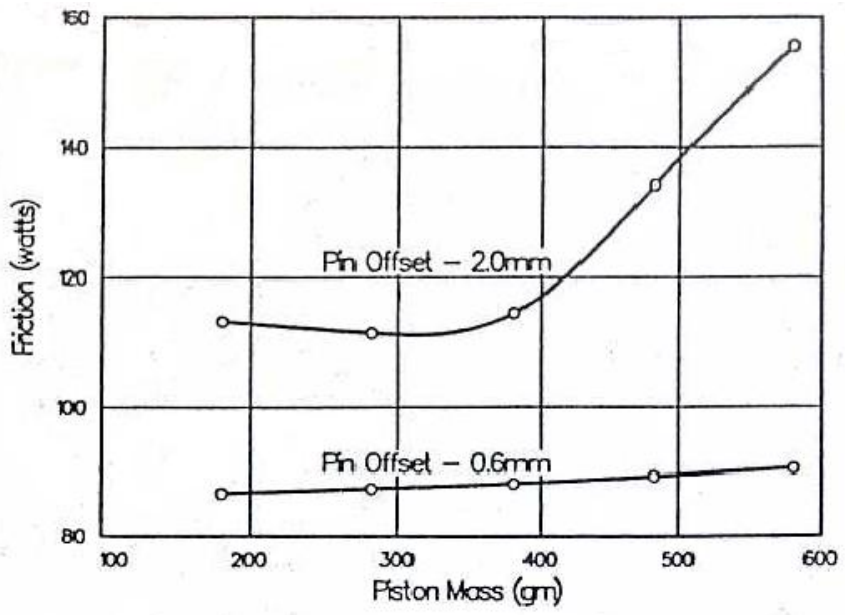

Figure 1.5 Effect of piston mass on piston friction for two different pin offsets (Goenka, P. K and Meernik, P. R [10])

In the paper of Keribar and Dursunkaya [12] that is continuation of [11] a comprehensive model of piston is developed for use in conjunction with piston secondary dynamic analysis to characterize the effects of the skirt-cylinder oil film on piston motions. For the Reynolds' equation a finite difference solution is used and an asperity contact model is implemented to the solution to calculate the oil and contact pressure distribution in the skirt-bore oil film as a function of all input design parameters and positions and motions of the skirt relative to the

cylinder. Figure 1.7 shows oil pressure distributions on the thrust and anti-thrust side of the skirt at selected crank angles during the compression and power strokes for the case of 1900 rpm and full load.

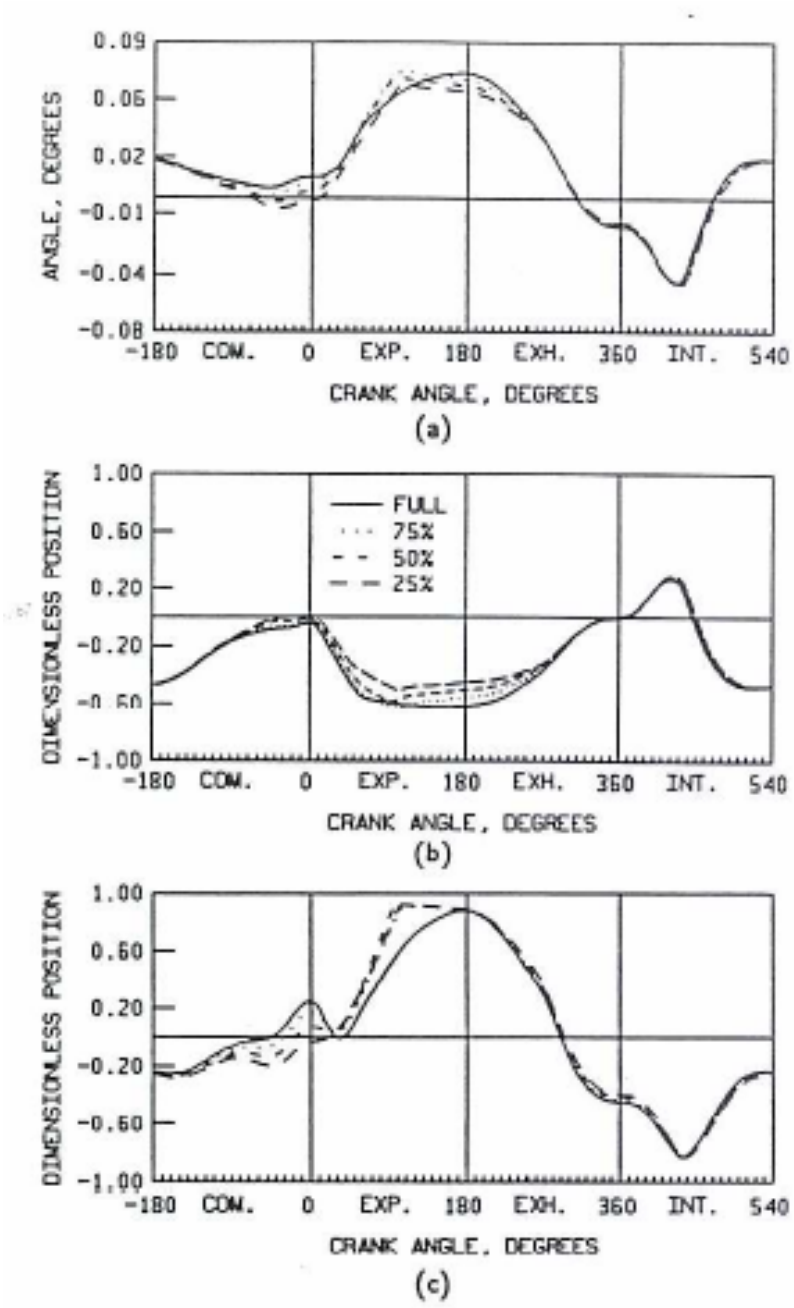

Figure 1.6 Effect of load on the skirt motion at 1900 rpm (a) rotational direction, (b) skirt top lateral direction, (c) skirt bottom lateral direction (Keribar, R. and Dursunkaya, Z [10])

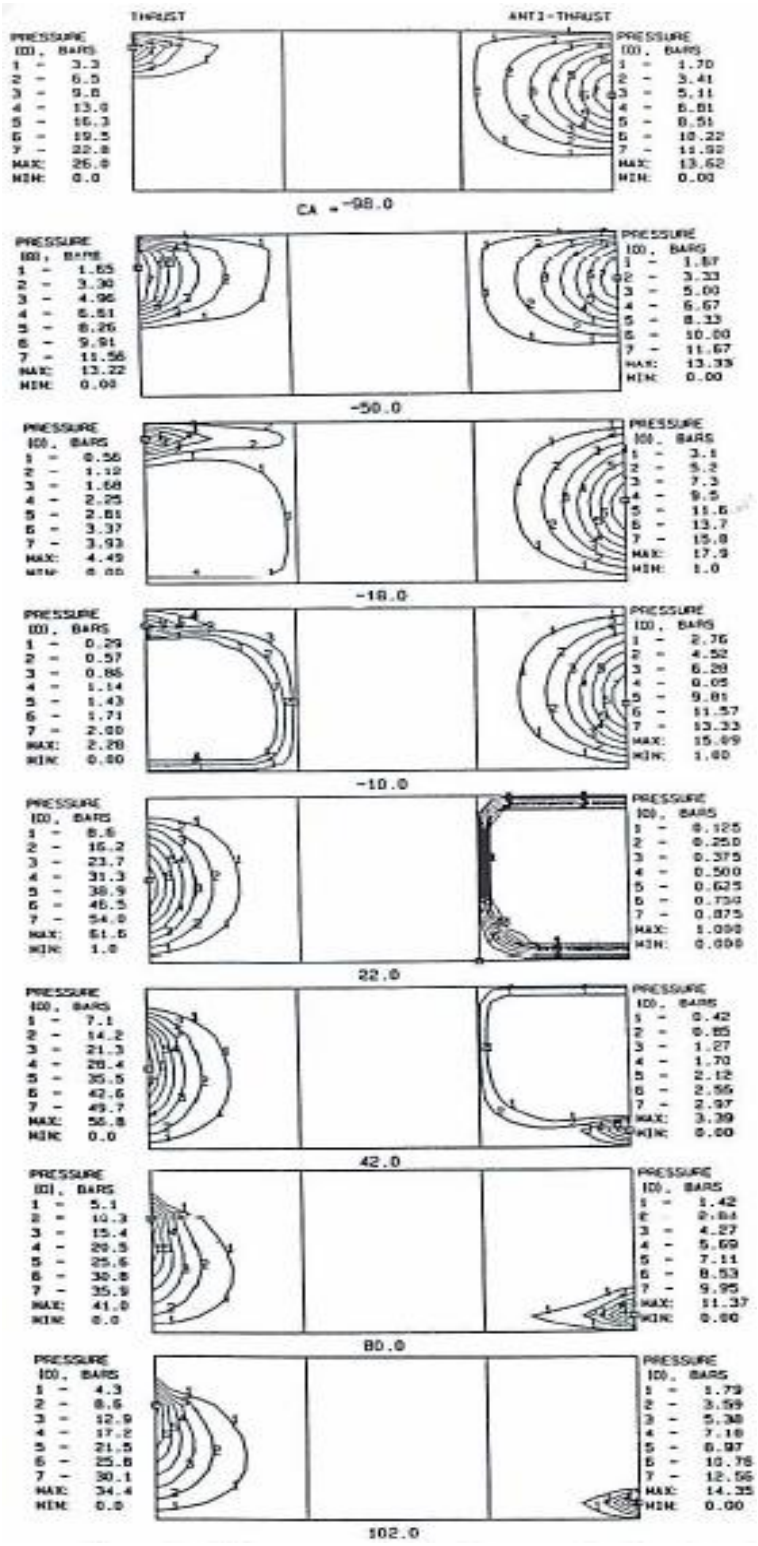

Figure 1.7 Oil pressure distributions on the thrust and anti-thrust side of the baseline skirt at selected crank angles during compression and power strokes, of case 1900 rpm full load (Keribar, R. and Dursunkaya, Z [10])

An integrated simulation methodology for the analysis of piston tribology is presented by Keribar, Dursunkaya and Ganapathy [13] that is comprised of coupled models of piston secondary dynamics, skirt oil film elasto-hydrodynamic lubrication and wristpin bearing hydrodynamics, developed earlier by the authors. The model predicts piston assembly secondary motions, piston skirt friction, skirt and wristpin oil film pressures, transient deformations, skirt-cylinder contact/impact pressures and skirt and cylinder wear loads. Figures 1.8 and 1.9 show cyclic variation of hydrodynamic and boundary friction forces and skirt radial deformation respectively.

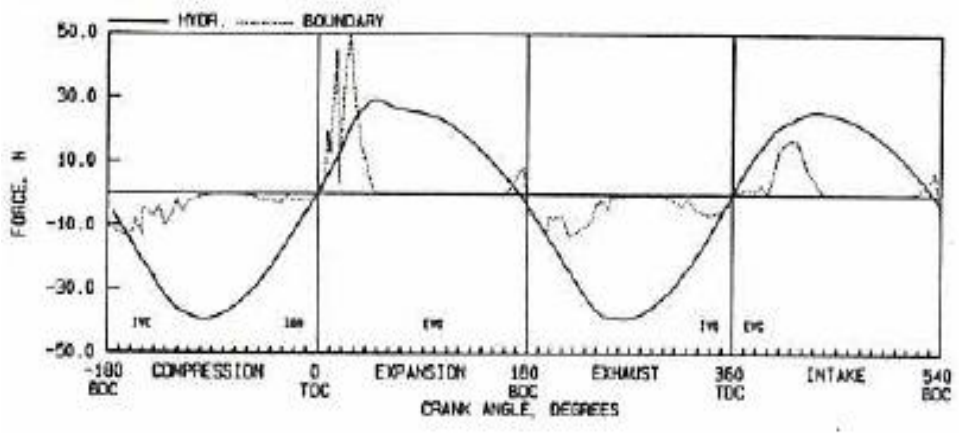

Figure 1.8 Cyclic variations of predicted skirt hydrodynamic and boundary friction force (Keribar, R., Dursunkaya, Z. and Ganapathy, V. [12])

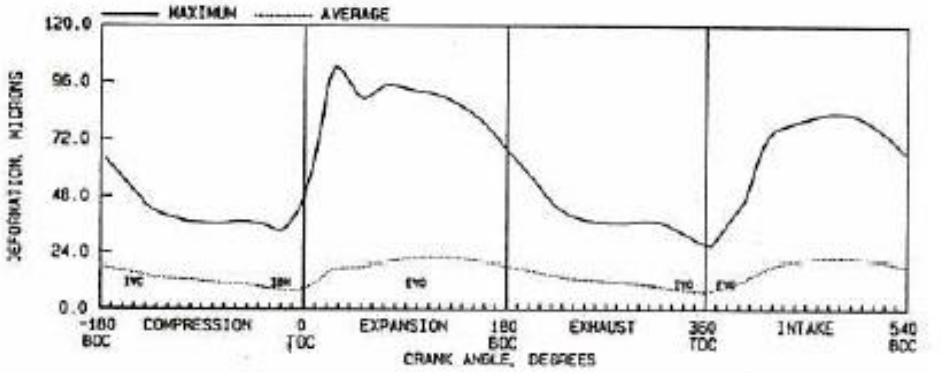

Figure 1.9 Cyclic variation of predicted maximum and average skirt radial deformation (Keribar, R., Dursunkaya, Z. and Ganapathy, V. [12])

In the field of lubrication of compressor bearings, Duyar and Dursunkaya [14, 15] solve elasto-hydrodynamic lubrication problem for compressor small end bearing using finite difference solution of the Reynolds' equation for elastic pin problem. With a parametric, study they search the effects of design parameters of the connecting rod small end bearing.

CHAPTER II

GOVERNING EQUATIONS

The differential equation governing the pressure distribution in fluid film lubrication in order to explain hydrodynamic lubrication mathematically is known as the Reynolds' equation. This equation was first derived in a remarkable paper by Osborne Reynolds in 1886. Reynolds restricted his analysis to an incompressible fluid. Harrison included the effects of compressibility. The Reynolds' equation can be derived in several ways with the assumptions;

1. Fluid incompressibility: Generally satisfactory for all single-phase liquids, but may not be so for gases or liquids containing gas bubbles.
2. Newtonian viscosity: Satisfactory for oils at low pressures, but less so at higher pressures.
3. Viscosity constant: Only even approximately true in mild conditions since viscosity is very dependent on both temperature and pressure variations.
4. Negligible inertia and turbulence: Generally satisfactory except at very high speeds or in very large bearings
5. Rigid solid surfaces: At high pressures or with compliant solids elastic deformation can make significant changes to geometry.
6. Pressure constant through thickness of film: Satisfactory in virtually all cases.
7. Smooth solid surfaces: Possibility of micro asperity hydrodynamic lubrication where surface asperities are not small compared to hydrodynamic film thickness.

Using the assumptions listed Standard Reynolds' Equation is derived by some simplifications of Navier Stokes' equations in association with continuity equation. The general form of Reynolds' equation for incompressible fluid for the configuration shown in Figure 2.1 is;

$$\frac{\partial}{\partial x}\left(h^3\frac{\partial P}{\partial x}\right)+\frac{\partial}{\partial y}\left(h^3\frac{\partial P}{\partial y}\right)=-6\mu U\frac{\partial h}{\partial x}+12\mu\frac{\partial h}{\partial t} \tag{2.1}$$

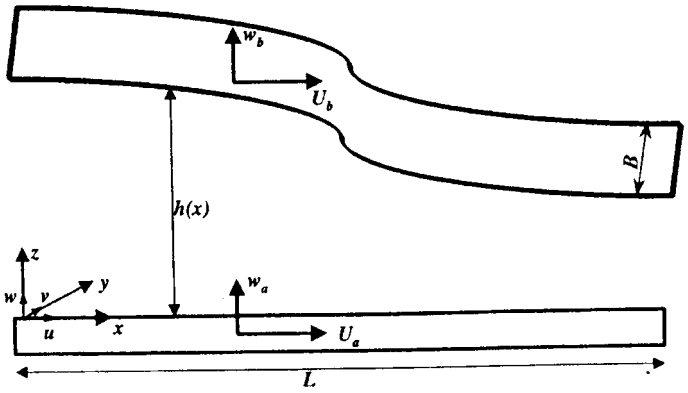

Figure 2.1 Coordinate system for equation (2.1)

2.1 Solution of Reynolds' Equation for Inclined Pad Bearing

To understand the secondary dynamics and lubrication of a piston it is useful to study the inclined pad bearing in advance. For an infinite width pad, the second term of equation (2.1) is neglected since pressure gradient in infinite y-direction is zero. For steady state condition the time derivative of film thickness on the right-hand side also drops. Hence the equation takes the form

$$\frac{d}{dx}\left(h^3\frac{dp}{dx}\right)=-6\mu U\frac{dh}{dx} \tag{2.2}$$

The film thickness in Figure 2.2 can be defined as;

$$h(x)=h_1-\frac{h_1-h_o}{E}x \tag{2.3}$$

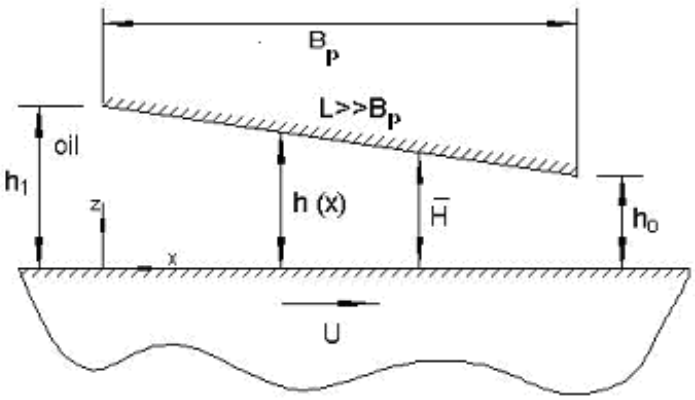

Figure 2.2 Inclined pad bearing

The equation (2.3) can be non-dimensionalized using; $H = \frac{h}{h_o}$, $X = \frac{x}{B_p}$, $H_1 = \frac{h_1}{h_o}$, $P = \frac{p}{6U\mu \frac{B_p}{h_o^2}}$, to get

$$\frac{d}{dX}\left(H^3 \frac{dP}{dX}\right) = \frac{dH}{dX} \tag{2.4}$$

The analytic solution of equation is straightforward using the boundary conditions,

$$P(X = 0) = 0$$
$$P(X = 1) = 0$$

The following form of non-dimensional pressure distribution as a function of non-dimensional X length is obtained

$$P(X) = \frac{(H_1 - 1)^2}{(H_1^2 - 1)} \cdot \frac{X(1 - X)}{H(X)^2} \tag{2.5}$$

2.2 Standard Reynolds' Equation:

The equation of the piston hydrodynamic lubrication problem is the Reynolds' equation for the film thickness and oil film pressure distribution. The following form of the Reynolds equation is used, where θ is the circumferential coordinate of the coordinate system given in figure 2.3. R is piston radius and U is piston sliding velocity in axial z-direction.

$$\frac{\partial}{\partial z}\left(h^3 \frac{\partial P}{\partial z}\right)+\frac{1}{R^2}\frac{\partial}{\partial \theta}\left(h^3 \frac{\partial P}{\partial \theta}\right)=-6\mu U\frac{\partial h}{\partial z}+12\mu\frac{\partial h}{\partial t} \tag{2.6}$$

where $\theta = \frac{x}{R}$

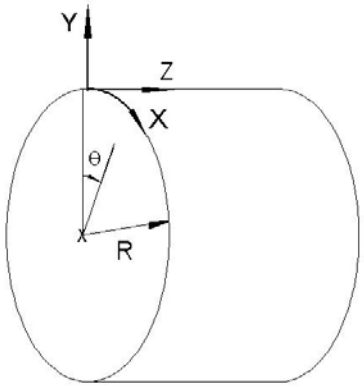

Figure 2.3 Coordinate system for equation (2.6)

2.3 Average Reynolds' Equation

When partial lubrication is present the texture of the asperity contacts affect the oil flow through the clearance of lubricating surfaces. An average Reynolds' equation for rough surface is defined to analyze roughness effects. The average Reynolds' equation is derived through flow simulation which is based on numerically solving the Reynolds' equation on a model bearing with a randomly generated surface roughness and then deriving the average Reynolds' equation from mean flow quantities.

$$\frac{\partial}{\partial z}\left(\phi_z h^3 \frac{\partial P}{\partial z}\right)+\frac{1}{R^2}\frac{\partial}{\partial \theta}\left(\phi_\theta h^3 \frac{\partial P}{\partial \theta}\right)=-6\mu U_z \frac{\partial \bar{h}_T}{\partial z}-6\mu . U_z \sigma \frac{\partial \phi_s}{\partial z}+12\mu \frac{\partial \bar{h}_T}{\partial t} \tag{2.7}$$

where, ϕ_z, ϕ_θ, ϕ_s are flow factors obtained by flow simulation.

Engineering surfaces have directional properties resulting from different manufacturing processes or because of running-in. These directional properties are mostly in the longitudinal or transverse directions. The contacts of a general three dimensional surface that is partially lubricated can be modeled as ellipses with the mean ellipticity ratio γ. Flow factors are dependent on ellipticity ratio and nominal film thickness.

Longitudinally oriented contact areas (γ>1), offer little resistance to the pressure flow, permitting only a small side flow. Since the average gap in the valleys is greater than the compliance, the resulting flow is greater than a smooth surface bearing.

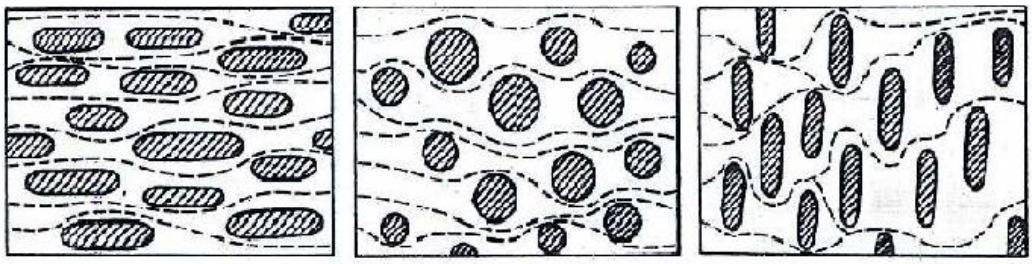

FFigure 2.4 Typical contact areas for (a) longitudinally oriented surface γ>1, (b) isotropic surface γ=1, and (c) transversely oriented surface γ<1 (Patir, N. and Cheng, H. S. [18])

For a given surface roughness characteristics, flow coefficients are calculated in Patir, N. and Cheng, H. S. [18,19] for the model problem shown in Figure 2.5.

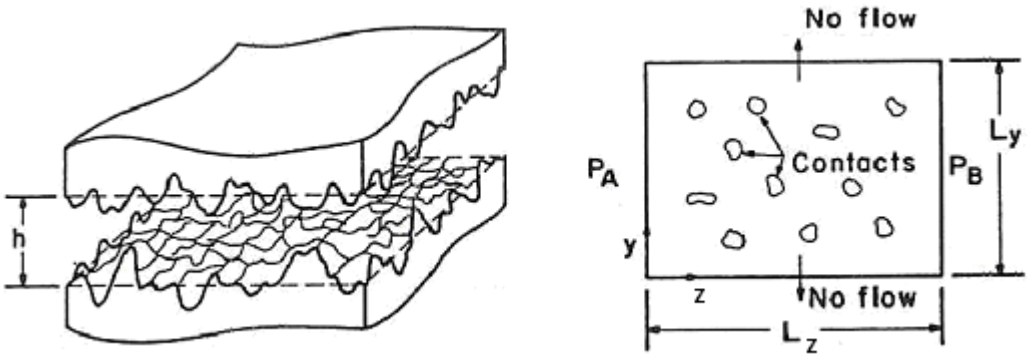

Figure 2.5 Model problem for simulation (Patir, N. and Cheng, H. S. [18])

$$\phi_z = \frac{\frac{1}{L_y}\int_0^{L_y}\left(\frac{h_T^3}{12\mu}\frac{\partial p}{\partial z}\right)dy}{\frac{h^3}{12\mu}\frac{\partial p}{\partial z}} \tag{2.8}$$

where

$$\frac{\partial p}{\partial z} = \frac{P_B - P_A}{L_z} \tag{2.9}$$

$$\phi_\theta = \phi_\theta(h,\ 1/\gamma) \tag{2.10}$$

$$\phi_s = \frac{2}{U_s\sigma}E\left(-\frac{h_T^3}{12\mu}\frac{\partial p}{\partial z}\right) \tag{2.11}$$

Detailed discussion for average Reynolds' equation is given by Patir, N. and Cheng, H. S [18,19].

CHAPTER III

MODELLING AND SOLUTION

The solution is carried only on the half side of the piston due to symmetry. The piston is symmetric with respect to x-z plane as shown in Figure 3.1. Using symmetry decreases the CPU time and accuracy increases as same mesh size describes a smaller region, resulting in a finer mesh size. The thrust and anti-thrust sides are defined for the opposing piston areas as shown in Figure 3.2.

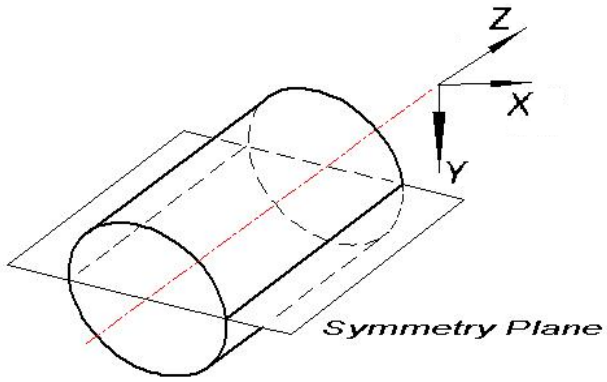

Figure 3.1 Symmetry plane of the piston

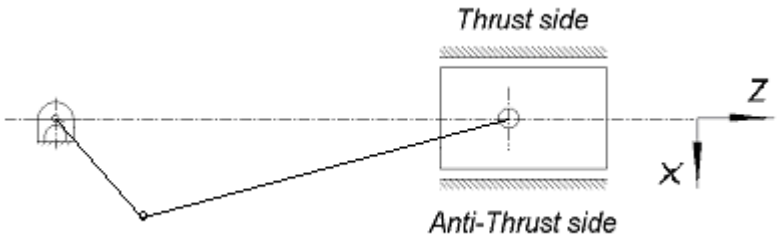

Figure 3.2 Thrust and anti thrust sides of a reciprocating piston

3.1 Solution of Reynolds' Equation

Reynolds' equation is solved numerically for calculation of film thickness and pressure distribution profiles. The second order derivatives are discretized using finite difference formulation for a selected mesh size of the lubricated regions of the thrust and anti-thrust planes on the piston. The pressure and the film thickness matrix of the finite difference mesh given in Figure 3.3 and Figure 3.4 are converted into single dimension arrays;

$$P_{i,j} = P_k \tag{3.1}$$

$$h_{i,j} = h_k \tag{3.2}$$

For a finite difference mesh with dimensions of *n* points in axial direction, and *m* points in circumferential direction for both thrust and anti-thrust lubricated domains the Reynolds' equation can be written as;

$$\begin{aligned}
&\frac{(h_{k+1}+h_k)^3}{8(\Delta z)^2}P_{k+1} + \frac{(h_k+h_{k-1})^3}{8(\Delta z)^2}P_{k-1} - \frac{(h_{k+1}+h_k)^3+(h_k+h_{k-1})^3}{8(\Delta z)^2}P_k \\
&+ \frac{(h_{k+m}+h_k)^3}{8(R\Delta\theta)^2}P_{k+m} + \frac{(h_k+h_{k-m})^3}{8(R\Delta\theta)^2}P_{k-m} - \frac{(h_{k+m}+h_k)^3+(h_k+h_{k-m})^3}{8(R\Delta\theta)^2}P_k \\
&= -6\mu U\frac{h_{k+1}+h_{k-1}}{2\Delta z} + 12\mu\frac{h_{k+1}+h_k^{old}}{\Delta t}
\end{aligned} \tag{3.3}$$

where h^{old} is the film thickness in the previous time step.

The solution is done according to the assumption that areas on the both sides of the piston where there exist the wristpin on the piston and the pin assembly slot on cylinder hole, shown in figure 1.4, are not lubricated. These not lubricated area, assumed to be defined by an 80˚ angle at center of piston divide the piston to two parts, thrust and anti thrust sides. Hence at one half of the piston 50˚ lubricated

thrust side and 50˚ lubricated anti thrust side are used as double patch solution areas illustrated in Figure 3.3 and Figure 3.4.

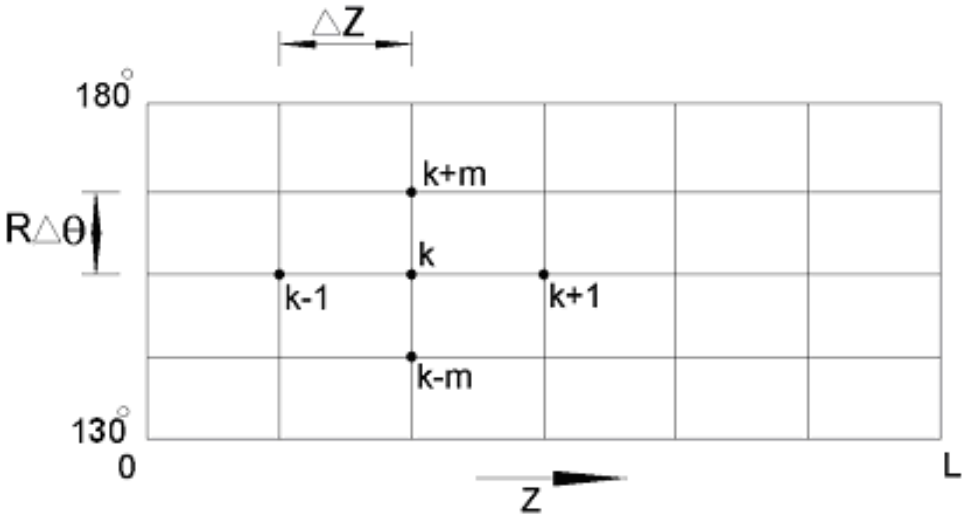

Figure 3.3 Lubricated anti thrust plane

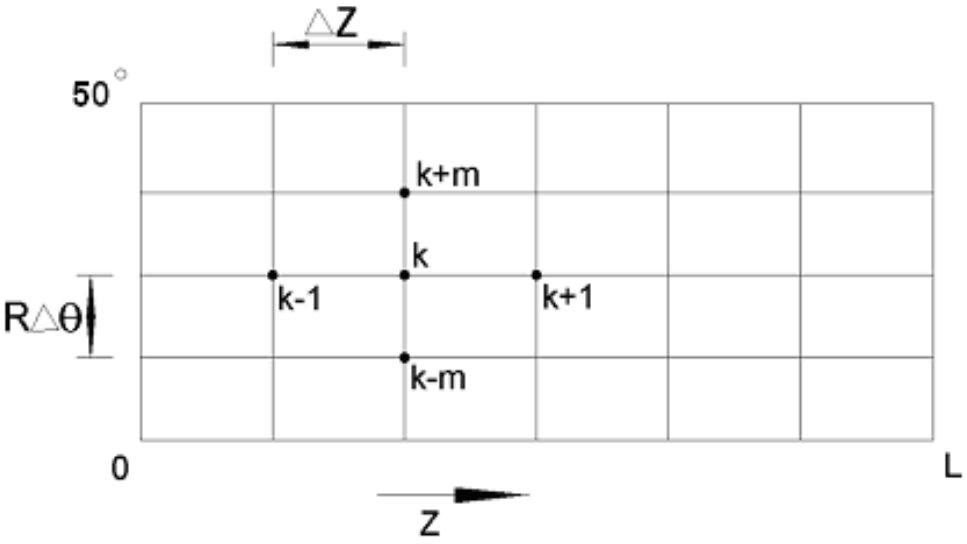

Figure 3.4 Lubricated thrust plane

Another approached used to define the lubricated area is to assume that all area that covers the piston is lubricated; hence a single solution patch shown in Figure 3.5 is used.

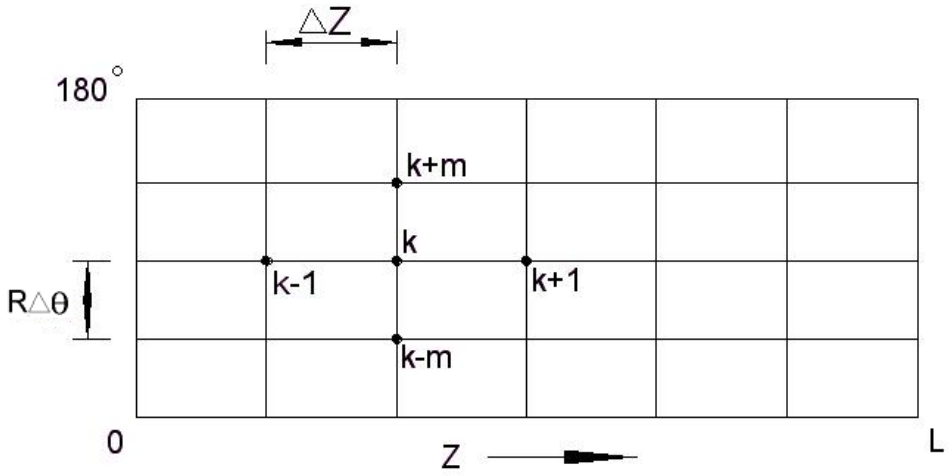

Figure 3.5 Single patch solution area

The film thickness h includes the effect of connecting rod motions, bearing clearance and oil feed groove.

$$h(z,\theta,t) = h_{dyn}(z,\theta,t) + h_{grv}(z,\theta,t) \tag{3.4}$$

$$h_{dyn}(i,j) = c + (e + \Delta z.j\tan\lambda)\cos\theta \tag{3.5}$$

where c is radial clearance, e is eccentricity at piston center of mass, λ is piston tilt angle and θ is circumferential coordinate. The film thickness matrix is written as a single dimensional array using equation (3.2).

The boundary conditions for the solution of the lubrication equations are as following,

$$P = P_{sc}\ ;\ z = 0 \tag{3.6}$$

$$P = P_{gas}\ ;\ z = L \tag{3.7}$$

$$P = \frac{(P_{gas} - P_{sc})}{L_h} z \; ; \; \theta = 50^\circ, \, 130^\circ \tag{3.8}$$

where, P_{sc} is the suction pressure inside the shell of the compressor, P_{gas} is the cylinder absolute gas pressure, L is the piston length, L_h is the length from piston head to groove. The linear distribution is considered only between the groove and piston head for the grooved piston at $\theta = 50^\circ, \, 130^\circ$. Remaining pressures at these boundaries are taken as suction pressure.

In the cavitation region of the bearing, Half Sommerfeld assumption is used [17],

$$P = 0, \quad \text{if } P < 0 \tag{3.9}$$

3.2 Solution of Average Reynolds' Equation

The average Reynolds' equation is solved with the same boundary conditions given for standard Reynolds' equation given in (3.6), (3.7) and (3.8); and similar film thickness profile given in (3.4) and (3.5) for given mesh size in the thrust and anti thrust regions. The discretized form of equation (2.7) using finite difference formulation is;

$$\begin{aligned}
&\frac{(\phi_{z\,k+1} + \phi_{z\,k})(h_{k+1} + h_k)^3}{16(\Delta z)^2} P_{k+1} + \frac{(\phi_{z\,k} + \phi_{z\,k-1})(h_k + h_{k-1})^3}{16(\Delta z)^2} P_{k-1} \\
&- \frac{(\phi_{z\,k+1} + \phi_{z\,k})(h_{k+1} + h_k)^3 + (\phi_{z\,k} + \phi_{z\,k-1})(h_k + h_{k-1})^3}{16(\Delta z)^2} P_k \\
&+ \frac{(\phi_{\theta\,k+m} + \phi_{\theta\,k})(h_{k+m} + h_k)^3}{16(R\Delta\theta)^2} P_{k+m} + \frac{(\phi_{\theta\,k} + \phi_{\theta\,k-m})(h_k + h_{k-m})^3}{16(R\Delta\theta)^2} P_{k-m} \\
&- \frac{(\phi_{\theta\,k+m} + \phi_{\theta\,k})(h_{k+m} + h_k)^3 + (\phi_{\theta\,k+m} + \phi_{\theta\,k})(h_k + h_{k-m})^3}{16(R\Delta\theta)^2} P_k \\
&= -6\mu U \frac{h_{k+1} + h_{k-1}}{2\Delta z} - 6\mu U \frac{\phi_{s\,k+1} + \phi_{s\,k-1}}{2\Delta z} + 12\mu \frac{h_{k+1} + h_k^{old}}{\Delta t}
\end{aligned} \tag{3.10}$$

The flow coefficients for equation (3.10) are calculated from equations. Numerical calculation of flow and shear flow coefficients is given in (Patir, N. and Cheng, H.S. [18, 19])

$$\phi_z = 1 - Ce^{-rH} \quad \text{for } \gamma \le 1 \tag{3.11}$$

$$\phi_z = 1 + Ce^{-r} \quad \text{for } \gamma > 1 \tag{3.12}$$

where H = h / σ. The constants *C* and *r* are given as functions of γ in Table 3.1.

For surface roughness with a given γ value, ϕ_θ is equal to the ϕ_z value corresponding to 1/ γ, i.e.

$$\phi_\theta(H,\gamma) = \phi_z(H,1/\gamma) \tag{3.13}$$

Table 3.1 Coefficients of equations (3.11) and (3.12) (Patir, N. and Cheng, H.S. [18])

γ	C	r	Range
1/9	1.48	0.42	H>1
1/6	1.38	0.42	H>1
1/3	1.18	0.42	H>0.75
1	0.90	0.56	H>0.5
3	0.225	1.5	H>0.5
6	0.520	1.5	H>0.5
9	0.870	1.5	H>0.5

The shear flow coefficint is calculated numerically from equation (2.10) and are presented in the form;

$$\phi_s = A_1 H^{\alpha_1} e^{-\alpha_2 H + \alpha_3 H^2} \quad \text{, for H} \le 5 \tag{3.14}$$

$$\phi_s = A_2 e^{-0.25H} \quad \text{, for H} > 5 \tag{3.15}$$

where H = h / σ and coefficients A_1, A_2, α_1, α_2, α_3 are listed as functions of γ in Table 3.2.

Table 3.2 Coefficients of equations (3.14) and (3.15) (Patir, N. and Cheng, H.S. [19])

γ	A_1	α_1	α_2	α_3	A_2
1/9	2.046	1.12	0.78	0.03	1.856
1/6	1.962	1.08	0.77	0.03	1.754
1/3	1.858	1.01	0.76	0.03	1.561
1	1.899	0.98	0.92	0.05	1.126
3	1.560	0.85	1.13	0.08	0.556
6	1.290	0.62	1.09	0.08	0.388
9	1.011	0.54	1.07	0.08	0.295

3.3 Average Shear Stress

Empirical shear stress factors ϕ_{fp} and ϕ_{fs} are defined by Patir, N. and Cheng, H.S. [19] such that the mean hydrodynamic shear stress is given in terms of mean quantities;

$$\bar{\tau} = \frac{\mu U}{h}(\phi_f \pm \phi_{fs}) \pm \phi_{fp} \cdot \frac{h}{2}\frac{\partial p}{\partial x} \tag{3.16}$$

where, the plus and minus signs are for the sliding and stationary surfaces respectively.

The ϕ_f term arises from averaging the sliding velocity component of the shear stress and can be obtained by integration the roughness heights for a given frequency density function. The equations are given by Patir, N. and Cheng, H.S. [18] and also the correction factor ϕ_{fs} for mean pressure flow component of the

average shear stress through simulation are discussed and the data are fitted into empirical relations of the form;

$$\phi_{fp} = 1 - De^{-sH} \tag{3.17}$$

where *s* and *D* are given as functions of γ in Table 3.3

Table 3.3 Coefficients of equation (3.17) (Patir, N. and Cheng, H.S. [19])

γ	**D**	**s**	**Range**
1/9	1.51	0.52	H>1
1/6	1.51	0.54	H>1
1/3	1.47	0.58	H>1
1	1.40	0.66	H>0.75
3	0.98	0.79	H>0.5
6	0.97	0.91	H>0.5
9	0.73	0.91	H>0.5

The term ϕ_{fs} is a correction factor for the combine effect of roughness and sliding, similar to ϕ_s. Its derivation is described in [19]. However when both surfaces have the same roughness structure $\phi_{fs} = 0$**,** since the piston and cylinder roughness values are close to each other, they are assumed to be equal in the calculations.

From equation (3.16) it is clear that two rough bearing surfaces are subjected to different shear stresses. The resultant difference in the friction force is balanced by additional horizontal force due to local pressure. In rough bearings, even for nominally parallel surfaces, the normal pressure acting on the sides of the asperities and valleys results in a net horizontal force. Detailed description of average shear stress can be found in reference [19].

3.4 Boundary Contact Model

During operation, surfaces may come close to each other so that asperity contacts occur or the surfaces may touch resulting in a boundary force created by the asperity contact pressures. In this case, boundary lubrication occurs and the load on the bearing is not only carried by the hydrodynamic force but also by the boundary force that is quantified using a microcontact model. Microcontact models are useful for interpreting roughness characteristic of two interfacing rough surfaces in such terms as the mean real area of contact, the contact density, the mean real pressure and the density of real contacts [19, 20].

The model of Greenwood and Trip, [21] is used for the calculation of boundary contact forces at the asperity contact regions of the finite difference mesh.

The boundary pressures are calculated on each node of the mesh using the equations,

$$P_{ci,j} = \frac{16\sqrt{2}}{15}\pi(\sigma\eta\zeta)^2 E\frac{\sqrt{\sigma}}{\sqrt{\zeta}}F\left(h_{i,j}/\sigma\right) \tag{3.18}$$

and

$$F(x) = \int (s-x)^{5/2} e^{(-s^2/2)} ds \tag{3.19}$$

where, parameters such as asperity density η, radius of curvature of asperity tops ζ, asperity heights σ, and composite elastic modulus E for the contacting material pairs, are the surface characteristics considered by the statistical model.

3.5 Wear Model

Wear is the progressive damage, involving material loss, which occurs on the surface of a component as a result of its motion relative to the adjacent working parts. It is the almost inevitable companion of the boundary friction. The wear rate

of a rolling or sliding contact is usually defined as the volume of material lost from the wearing surface per unit sliding distance and is investigated with the Archard wear equation (Archard, J., F. [22]);

$$\varpi = k\frac{W}{Hr} \tag{3.20}$$

where, ϖ is the wear rate in volume per distance, W is the wear load [N], Hr is the hardness of the sliding material in Pa, U is the sliding speed [m/s]. The dimensionless constant k is known as the wear coefficient and its value is vital in application of equation (3.19). The constant k is difficult to obtain but for comparative study it is important to hold it constant for the all parametric work.

For the calculation of the wear rate the following equation is used in the code which gives wear of volume of material per second;

$$WearRate.\left[m^3/\sec\right] = k\frac{\frac{1}{T}\int_0^T \int_A P_c U dA.dt}{Hr.9.81x10^6} \tag{3.21}$$

where T is the period of 360˚ crank rotation. The contact pressure is calculated using the boundary contact model using equation (3.18).

3.6 Power Loss

Hydrodynamic power loss which is related to viscous friction of the lubricant and boundary power loss due to boundary contact friction are calculated using the following equations. For hydrodynamic power loss;

$$\mathrm{IP}_{hyd} = \int_A \tau.UdA \tag{3.22}$$

where, for standard Reynolds' equation shear stress is found using:

$$\tau = \mu \frac{\partial U}{\partial y} = \mu \frac{U}{h} \tag{3.23}$$

however, for average Reynolds' equation applications, equation (3.16) is used for calculation of average shear stress.

For boundary power loss;

$$\mathrm{IP}_{bdy} = \int_A f.P_c.U.dA \tag{3.24}$$

where f is the friction coefficient, U is the sliding velocity and P_c is the boundary contact pressure calculated using equation (3.18).

3.7 Slider – Crank Dynamics

Piston dynamics parameters such as piston axial velocity, piston axial acceleration, piston inertial behavior versus crank rotational speed, are solved after analyzing the slider crank mechanism.

Crank angle α is taken positive in the clock wise direction, and β is positive when the crank pivot A is in the anti-thrust side and negative when A is in the thrust side in Figure 3.6.

The relation between angles α and β can be written as follows;

$$s + h_m \sin(\alpha) = l \sin(\beta) \tag{3.25}$$

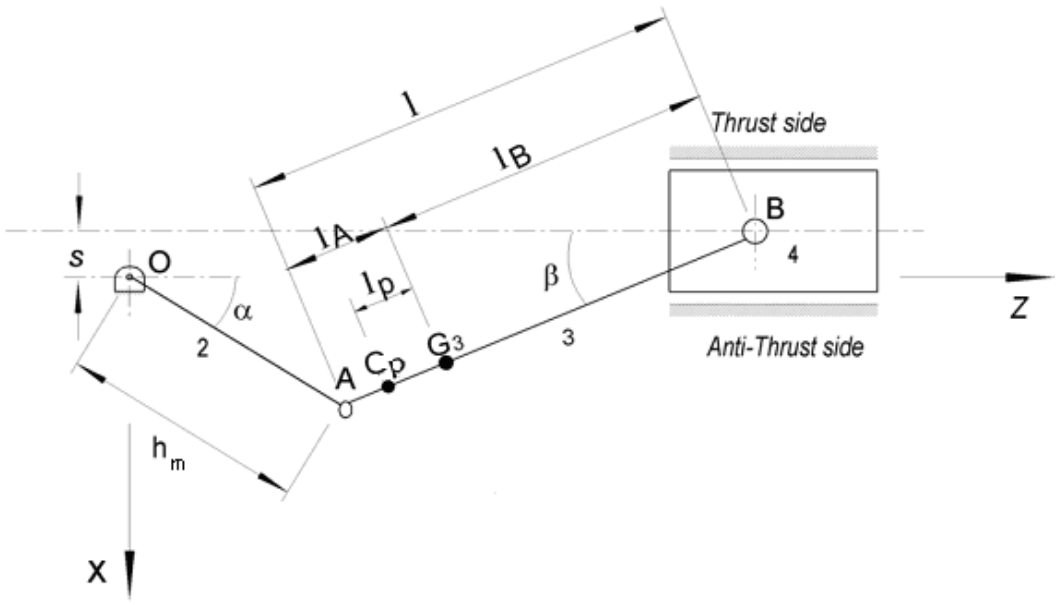

Figure 3.6 Slider crank mechanism

where *s* is the misalignment between cylinder axis and crank axis of rotation, *h* is the eccentricity of the crank, *l* is length of connecting rod. The angle β that is the angle between connecting rod and cylinder axis is obtained by rearranging equation (3.25):

$$\beta = \sin^{-1}\left(\frac{s + h_m \sin(\alpha)}{l}\right) \tag{3.26}$$

The connecting rod angular velocity and acceleration are obtained by differentiating equation (3.25) with respect to time once for angular velocity, and twice for angular acceleration;

$$\dot{\beta} = \frac{h_m}{l}\frac{\cos\alpha}{\cos\beta}\omega \tag{3.27}$$

$$\ddot{\beta} = \frac{l\sin\beta\dot{\beta}^2 - h_m\omega^2\sin\alpha}{b\cos\beta} \tag{3.28}$$

The piston pin axial position in Figure 3.5 is found by,

$$z = h_m \cos\alpha + l\cos\beta \tag{3.29}$$

Equation (3.29) is differentiated once and twice with respect to time to obtain piston axial velocity and acceleration respectively,

$$\dot{z} = -\omega h_m \sin\alpha - l\dot{\beta}\cos\beta \tag{3.30}$$

$$\ddot{z} = -\omega^2 h_m \cos\alpha - l\dot{\beta}^2 \sin\beta - l\ddot{\beta}\cos\beta \tag{3.31}$$

3.8 Equivalent Masses

The effect of connecting rod inertia force can be easily analyzed by concentrating a portion the connecting rod mass at the crank pin A and the remaining mass at the wristpin B (Figure 3.5). The reason for this is that the crankpin moves on a circle and the wristpin on a straight line, however center of mass is somewhere between crankpin and wristpin and its motion is more complicated.

The connecting rod mass assumed to be concentrated at center of mass G_3 is divided into two parts; m_{3B} that is concentrated at the wristpin, and m_{3P} that is concentrated at center of percussion C_p. Dynamic equivalence to the original case is procured if; the total mass, position of center of gravity G_3 and the moment of inertia are same with the original.

$$m_3 = m_{3B} + m_{3P} \tag{3.32}$$

$$m_{3B} l_B = m_{3P} l_P \tag{3.33}$$

$$I_G = m_{3B} l_B^2 + m_{3P} l_p^2 \tag{3.34}$$

The portion of the mass concentrated at each point is calculated by solving equations (3.32) and (3.33);

$$m_{3B} = m_3 \frac{l_P}{l_B + l_P} \tag{3.35}$$

$$m_{3P} = m_3 \frac{l_B}{l_B + l_P} \tag{3.36}$$

Substituting equations (3.35) and (3.36) into (3.34) gives

$$I_G = m_3 \frac{l_P}{l_B + l_P} l_B^2 + m_3 \frac{l_B}{l_B + l_P} l_p^2 = m_3 l_P l_B \tag{3.37}$$

or, $$l_P l_B = \frac{I_G}{m_3} \tag{3.38}$$

From equation (3.38) it is clear that the distances l_P and l_B depend on each other. In the usual connecting rod, the center of percussion is close to the crankpin and it is assumed that they are coincident. Thus when $l_A = l_P$, equations (3.35) and (3.35) take the form

$$m_{3B} = m_3 \frac{l_A}{l} \tag{3.39}$$

and

$$m_{3P} = m_3 \frac{l_B}{l} \tag{3.40}$$

3.9 Kinetics

The piston side force on cylinder wall, is calculated form slider-crank dynamics for a given cylinder pressure profile including the effect of moving parts inertias by locating equivalent mass at wristpin;

$$m_B = m_{3B} + m_4 \tag{3.41}$$

$$F_{Z_{34}} = -(m_B \ddot{z} + F_{gas}) \tag{3.42}$$

Substituting equation (3.41) into (3.42)

$$F_{X_{34}} = -\left\{\left(m_{3b} + m_4\right) \cdot \ddot{z} + F_{gas}\right\} \cdot \tan\beta \tag{3.43}$$

Detailed slider-crank analyze is at Shigley, J. E. and Uicker, J.J. [23]

3.10 Numerical Solution Method

The solution of lubrication problem of the piston-cylinder bearing requires simultaneous solutions of equations of motion in axial direction which are related with slider crank dynamics (equations (3.25)-(3.43)); and in lateral direction, that are related with secondary motion and lubrication of the piston (equations (3.3)-(.3.18)). The calculations are carried step by step for each crank angle for a compressor cycle consisting of suction and compression.

$$m_4 \ddot{\varepsilon}_{cm} = \sum F_x \tag{3.44}$$

where ε is the eccentricity of center of mass of the piston from cylinder axis as shown in Figure 3.7.

In lateral x-direction,

$$m_4 \ddot{z} = \sum F_z \tag{3.45}$$

in axial z-direction and

$$I_G \ddot{\alpha}_{tilt} = \sum M_y \tag{3.46}$$

in rotational direction where α_{tilt} is the angle between piston axis and cylinder axis as shown in Figure 3.7.

In equations (3.44), (3.45) and (3.46); m is piston mass, I_G is the piston moment of inertia at its center of mass, and z is axial coordinate. F and M are the force and moment applied on the piston at center of mass respectively.

The first step is determining the side force which is the force applied on the piston by the connecting rod in lateral direction and is the load to be carried by piston-cylinder bearing. Side force is calculated by solving the slider crank mechanism's dynamics and kinetics analytically for a given cylinder gas pressure using equations (3.25)-(3.43).

Knowing the side force lateral equation of motions, equations (3.45)-(3.46), force and moment balance, are solved numerically using Newton-Raphson method which requires the solution of Reynolds'/average Reynolds' equation.

The discretized finite difference form of Reynolds' equation is used for the numerical solution given with (3.3) for standard Reynolds' equation or (3.10) for average Reynolds' equation. The equations (3.3) or (3.10) can be written in matrix form;

$$\begin{bmatrix} a_{11} & a_{11} & \dots & a_{11} \\ . & . & \dots & . \\ a_{11} & a_{11} & \dots & a_{11} \end{bmatrix} \begin{bmatrix} P_1 \\ . \\ P_N \end{bmatrix} + \begin{bmatrix} b_{11} & b_{11} & \dots & b_{11} \\ . & . & \dots & . \\ b_{11} & b_{11} & \dots & b_{11} \end{bmatrix} \begin{bmatrix} h_1 \\ . \\ h_N \end{bmatrix} = \begin{bmatrix} F_{11} \\ . \\ F_{1_N} \end{bmatrix} \tag{3.47}$$

or,

$$A.\widetilde{P}_u + B\widetilde{h} = \widetilde{F}_1 \tag{3.48}$$

where $\widetilde{P}_u$ is the unknown internal grid pressure array, A is the coefficient matrix of pressures that contains coefficients of difference equations approximating the left hand side of the Reynolds' equation. Multipliers of difference formulae used for space and time derivatives of h on the right hand side of the Reynolds' equation make up matrix B. The right hand side term F_1 includes the effect of the known boundary pressures, contact pressures and the clearances h due to dynamics.

For a given film thickness the hydrodynamic pressure for each node of the mesh is solved using equation (3.48). The given film thickness profile is the result of given piston eccentricity and tilt angle. The boundary contact pressures are calculated form equation (3.18). Integrating the hydrodynamic and boundary pressures over the piston lubricated area the force and moments that are used in the equations of motion (3.44)-(3.46) are obtained.

The equations of motion describing the secondary dynamics in lateral plane can be treated as a set of nonlinear algebraic equations of the form

$$F_j(x_1, x_2, ..., x_m) = 0 \tag{3.49}$$

and are solved iteratively, using the Newton-Raphson method:

$$J_{ij}(x_i^{k+1} - x_i^k) = -F_j(x_1^k, x_2^k, ..., x_m^k) \tag{3.50}$$

where, J_{ij} denotes the Jacobian matrix $\partial F_j / \partial x_i$ and k is the iteration number. For convergence both convergence of variables, eccentricity and tilt angle, and convergence of functions, equations of motion, are required. The iteration is

considered converged when relative changes form iteration to iteration in variables x_i, and also relative functional residuals F_j are small. After convergence the calculations proceed with the next step that is the next angle. An outer cycle loop is used for cyclic convergence.

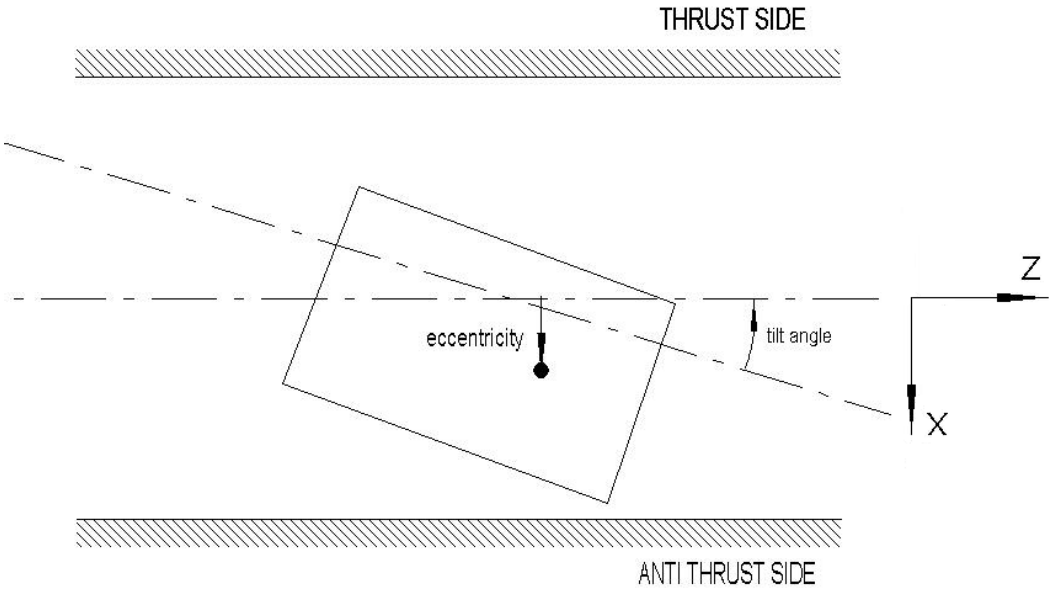

Figure 3.7 Piston tilt and eccentricity

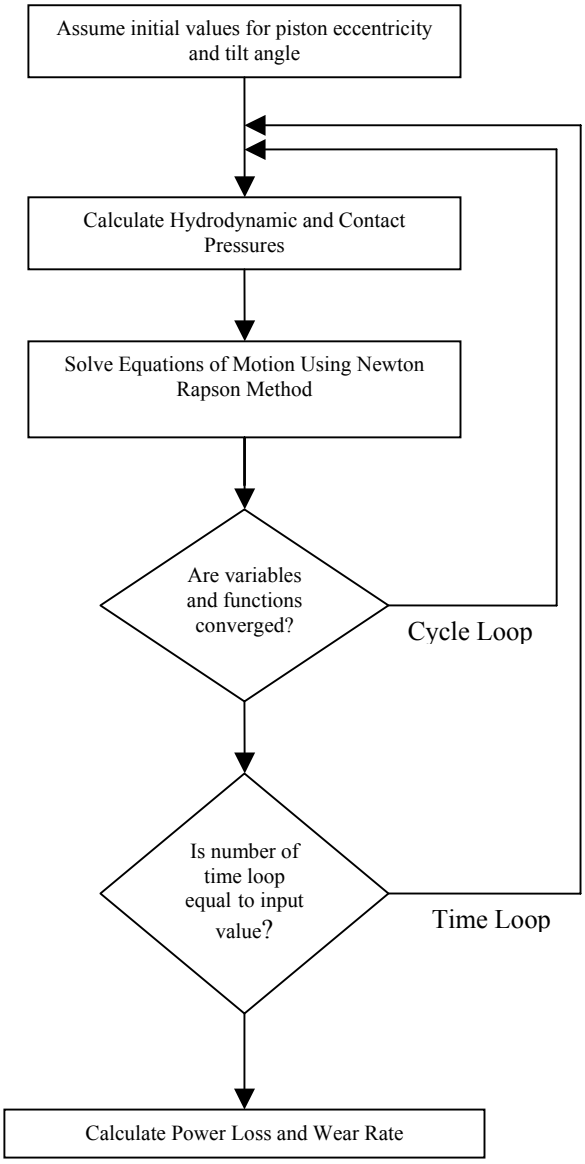

Figure 3.8 Numerical solution flow chart

CHAPTER IV

VERIFICATION OF THE MODEL

4.1 Comparison with the Inclined Pad Solution

When there is a few order of difference between length and width of a sliding surface infinite width assumption is valid since pressure gradient in length is zero. This situation is easily investigated from numeric results of the pressure profile.

The Reynolds' equation is solved numerically for an infinite with inclined pad bearing assumption. The results were compared with the analytic solution of the pad given in equation (2.5).

4.1.1 Input Parameters for the Inclined Pad

- Length of the bearing: 16.575 mm
- Width of the bearing: 8 m
- Kinematic viscosity: 0.001 Pa.s
- Sliding speed: 10 m/s
- h_1(Figure 2.2): 10 μm
- h_0(Figure 2.2): 5.02 μm

4.2.2 Results of Solutions

The pressure distributions for both numeric and analytic solutions are given in Figure 4.1. Despite using very rough mesh, the differences of the pressure distributions between the pressures at the nodes of the mesh and analytical curve

are small enough to conclude that the numeric solution of the Reynolds' equation is valid.

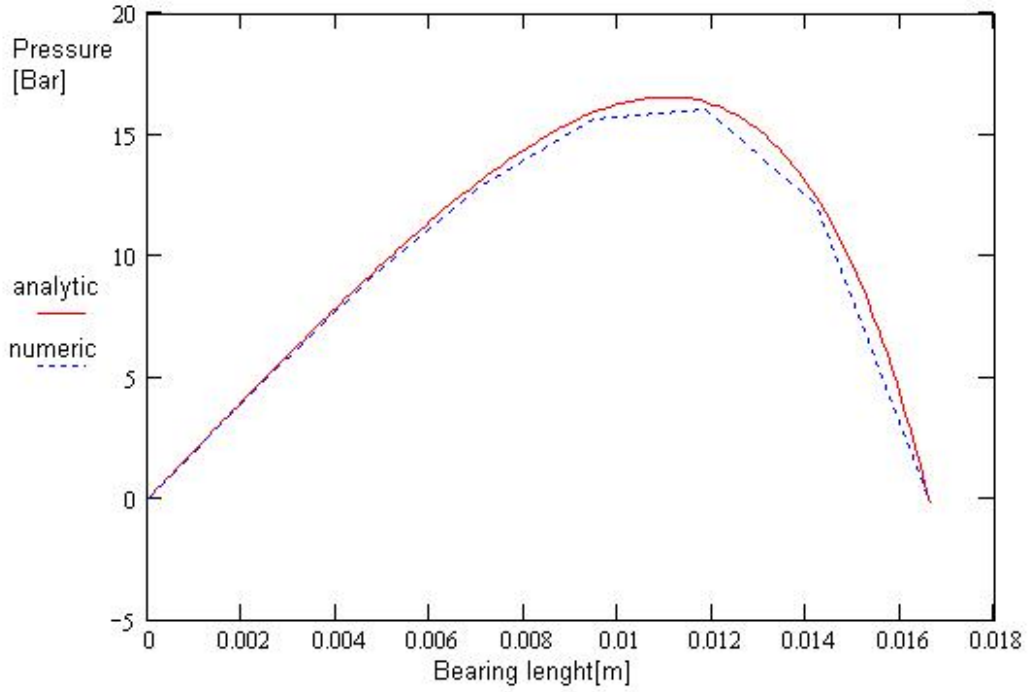

Figure 4.1 Analytic and numeric solutions for the infinite width inclined pad bearing

CHAPTER V

RESULTS AND DISCUSSIONS

5.1 Input Parameters

The base piston model is the piston of MTS 170 M type compressor. The PV data can be measured experimentally or calculated using commercial software and it is input data for the slider crank analysis. The PV data used is given in Figure 5.1. Other input parameters for the base piston model, are as follows;

- Piston diameter : 25.40 mm
- Piston axial length: 16.57 mm
- Piston mass : 0.031 kg
- Connecting rod mass: 0.027 kg
- Center of mass location from piston skirt in z-axis: 8.965 mm
- Wristpin location from piston skirt in z-axis: 6.665 mm
- Crank rotational speed: 3000 rpm
- Crank offset: 2.7 mm
- Crank eccentricity: 11.40 mm
- Connecting rod length: 47.00 mm
- Lubricant viscosity: 0.002 Pa.s
- Radial clearance : 3 μm
- Combined roughness: 0.36 μm
- Ellipticity ratio: 6
- Combined elastic modulus: 2.2×10^{11} Pa
- Suction pressure: 0.624 Bar
- Groove beginning location from skirt side end: 7.04 mm
- Groove width: 2.82 mm
- Mesh size, (axial)x(circumferential): 17x11

The mesh size of both thrust and anti thrust side is 17x11. So the whole lubricated area is simulated with a mesh size of 22x17, 22 in circumferential and 17 in axial direction.

When selecting the mesh number in axial direction, modeling the groove has to be considered. The groove can be simulated with at least three nodes. One node simulates the beginning of the groove, one the end and one is at the center. But this cause a big error in integration of the film pressure field, since only the point at the center of 2.82 mm wide groove has zero gage pressure. However the pressure around the whole groove is zero. Hence more than three nodes should define the groove.

It is important for the numeric calculations to use such a mesh size that $\Delta z / R\Delta\theta$ ratio is close to 1. Also the mesh density has to be high enough. The higher the mesh density, the more precise the result is. However, after a particular mesh size the solution is accurate enough and further increasing the mesh do not affects the result significantly. Also increasing mesh density also increases the CPU time. So an optimum mesh size is selected by considering precision and CPU time besides accurate simulation of the piston.

5.1.1 Input PV Data

PV data of a reciprocating compressor depends on piston stroke, piston diameter, suction and exhaust valve leave stiffness that determines the opening and closing crank angles of valves. The PV can be determined experimentally however, the studied MTS 170 M compressor is an ongoing design project so the numerical PV results of a commercial code under ASHRAE-T working conditions are used as input data. The Figure 5.1 shows the PV diagram used in computations. The refrigerant absolute gas pressure inside the cylinder is given as a function of crank angle in Figure 5.1.

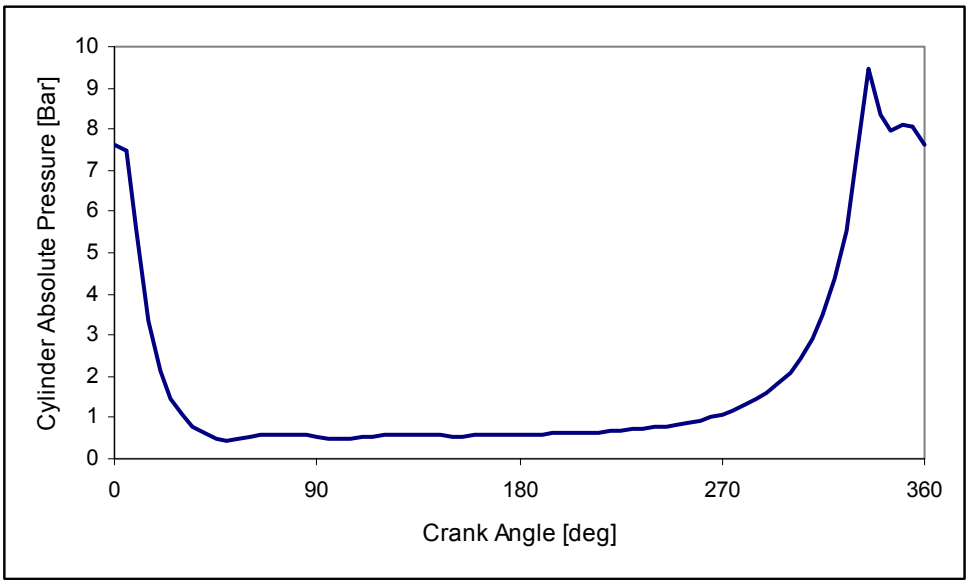

Figure 5.1 Absolute gas pressure inside cylinder versus crank angle diagram

5.1.2 Calculated Piston Side Force

Using the pressure data the piston side force for each crank angle that has to be carried on lubricated surfaces is calculated form the solution of slider crank dynamics using equations (3.25) - (3.43) for the coordinate system given in Figure 3.5. The calculated side force that is an input parameter for the lubrication problem and for equations of motion in lateral direction is given in Figure 5.2.

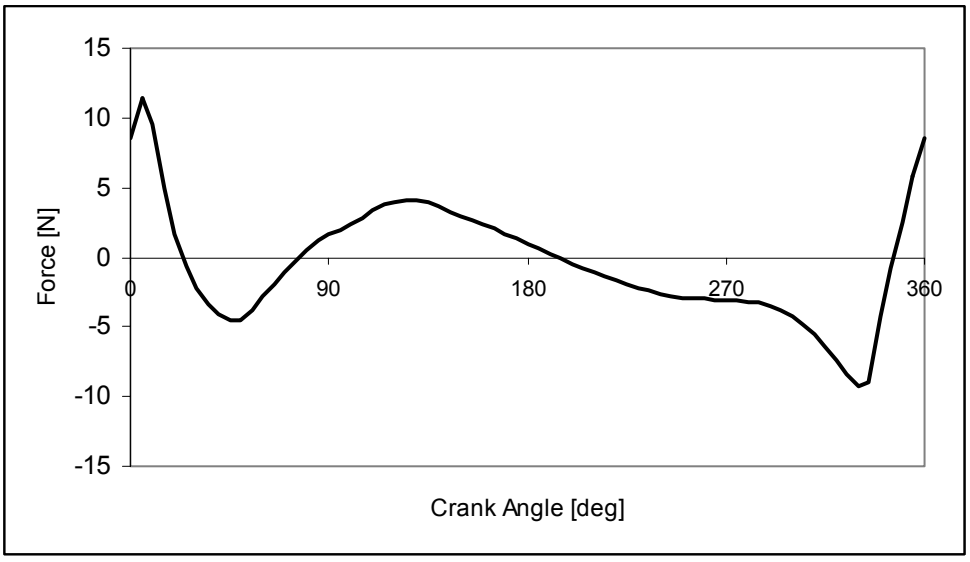

Figure 5.2 Piston lateral (side) force versus crank angle

5.2 Base Model Solution

The base piston model with groove is solved using the standard Reynolds' equation. The solution gives the eccentricity of the piston (Figure 3.6), at the center of mass that is shown in Figure 5.3; and the tilt angle (Figure 3.6) of the piston axis with respect to cylinder axis shown in Figure 5.4. For a cyclic convergence, at crank angles 0˚ and 360˚ the initial and final values of the solved parameters must be close to each other. It can be investigated form Figure 5.3 and Figure 5.4 that the eccentricity and tilt angle solutions have converged since the values at 0˚ and 360˚ are almost equal to each other.

Knowing these two parameters, the remaining piston dynamics can be solved since the power loss and wear rates are functions of film thickness and film thickness is function of piston tilt and eccentricity.

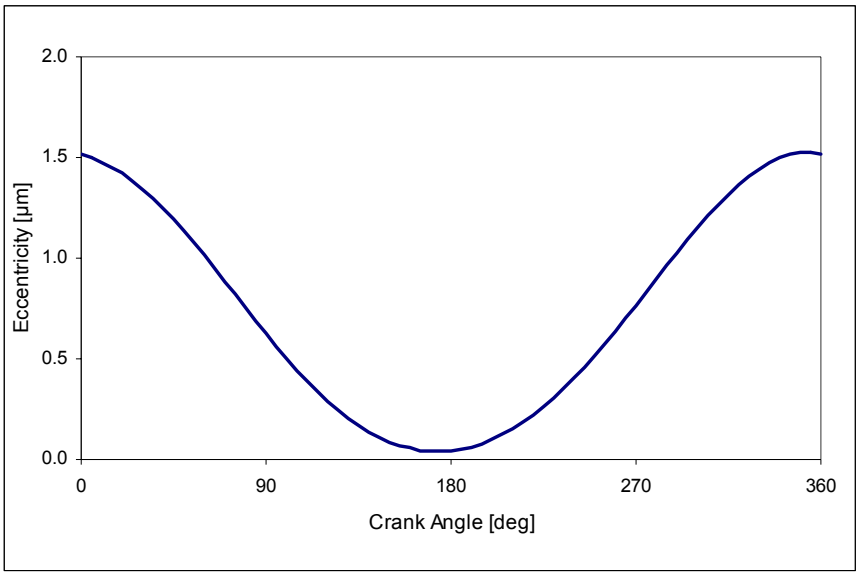

Figure 5.3 Eccentricity of center of mass from cylinder axis of the base piston model with respect to crank angle

After the solution of eccentricity and tilt angle, the code calculates using postprocessors, the minimum film thickness for each crank angle. To understand the piston dynamics film thicknesses of piston head thrust, skirt thrust, skirt anti thrust and head anti thrust sides are calculated and plot with respect to crank

angle. With head thrust side the closer point to the cylinder wall of the intersection of piston head and piston thrust side are determined. In Figure 5.5 this point is shown at top corner of the right hand side of the sketch of the piston. Similarly skirt thrust, head anti thrust and skirt anti thrust side determine the top left, bottom right and bottom left corners respectively. Boundary and hydrodynamic power losses and cycle wear rate are calculated knowing the film thickness between the piston and cylinder.

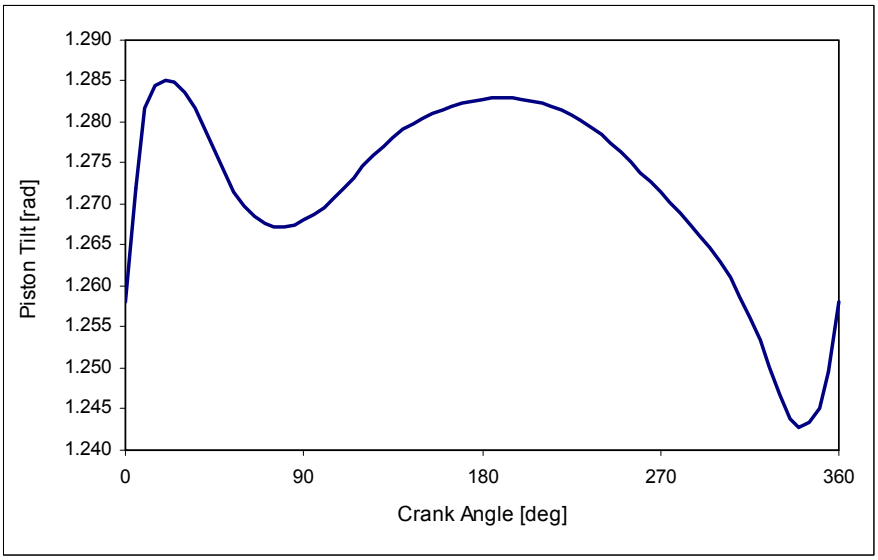

Figure 5.4 Tilt angle variation of the base piston model with respect to crank angle

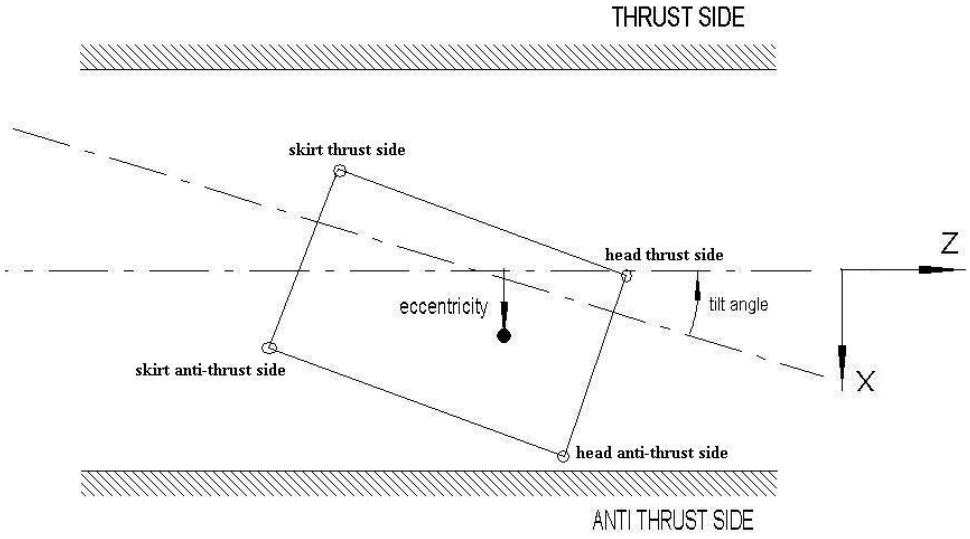

Figure 5.5 The position of base piston model

The piston works with positive eccentricity and positive tilt angle giving positions to piston similar to the sketch shown in Figure 5.5. Between crank angles 356˚-176˚ the piston moves with negative velocity in z-direction. Hence the wedge effect causes negative oil film pressure force in x-direction. In order to meet positive side force by creating a negative reaction force, eccentricity of the piston increases in positive x-direction and an additional negative oil film pressure reaction force is obtained because of the squeeze action. So in such a case the oil pressure forces of wedge effect and squeeze effect are in same direction. However to meet negative side force at crank angles about 30˚-80˚ the tilt angle decreases so with the squeeze action, the reaction force needed is created. Between these angles the wedge effect also causes additional negative force so the squeeze and wedge effect oil film forces are in opposite direction. In other words, squeeze action carries side load together with the negative oil film forces because of the wedge effect.

With a very small variation in tilt angle, since the clearance is very small, sufficient oil film force can be obtained. Thus, the reaction force needed can be created only by the squeeze effect alone.

Dominant side force acting on the piston is negative in x-direction between 180-360˚ crank angles and positive reaction force has to be created by lubrication dynamics. The piston velocity is positive in z-direction between crank angles 176˚-356˚, hence the wedge effect creates positive oil pressure force in x-direction. Piston eccentricity starts decreasing after 180˚ crank angle resulting in additional positive oil film force due to the squeezing action. But after crank angle about 340˚, the side load is positive. Positive side load and positive oil film force due to wedge is carried by the squeeze action resulting from the increase in tilt angle.

Figure 5.6 shows minimum film thickness with respect to crank angle and Figure 5.9 gives boundary and hydrodynamic power losses for given crank angle.

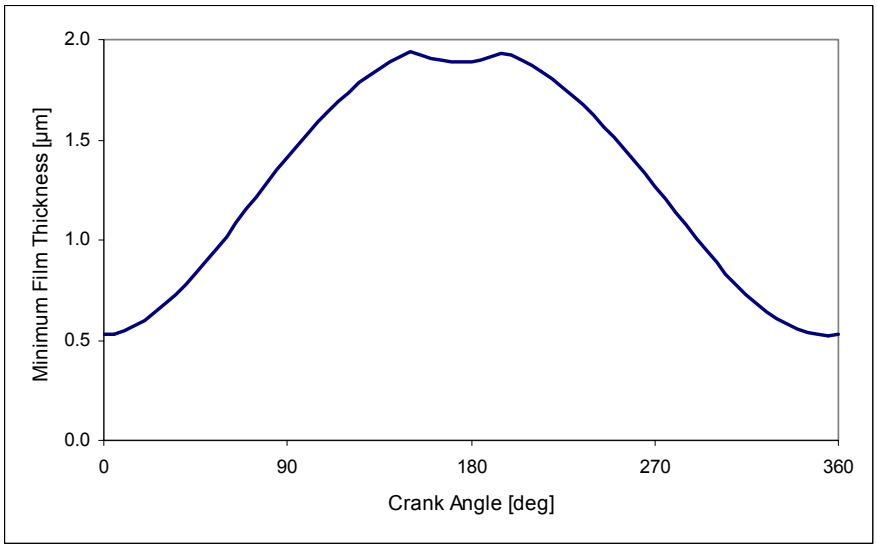

Figure 5.6 Minimum film thicknesses plot of the base piston model

If piston eccentricity and tilt angle values are different than zero, the minimum film thickness is one of the smallest of the piston skirt thrust or anti thrust side or piston head thrust or anti thrust side film thicknesses. Figure 5.6 shows the minimum film thickness of the base model.

The piston lubrication dynamics is better understood from the film thickness values of the piston skirt thrust and anti-thrust side and piston head thrust and anti thrust side film thickness plots. In given Figures 5.7 and Figure 5.8 skirt_t, skirt_at, head_t, head_at stand for skirt thrust side film thickness, skirt anti thrust side film thickness, head thrust side film thickness, head anti thrust side film thickness respectively. It is useful to give these film thicknesses in spite of giving tilt and eccentricity values since the piston position for a certain crank angle is easily covered knowing these film thicknesses.

In Figure 5.7 the thrust side film thicknesses are shown. The head side film thickness is higher than the skirt side. This is the result of positive tilt shown in Figure 5.4. The same effect is also present at anti-thrust side film thicknesses that are given in Figure 5.8. But here the skirt side film thicknesses are higher as expected. On the other hand the positive eccentricity causes higher film thickness values at thrust side than anti thrust side.

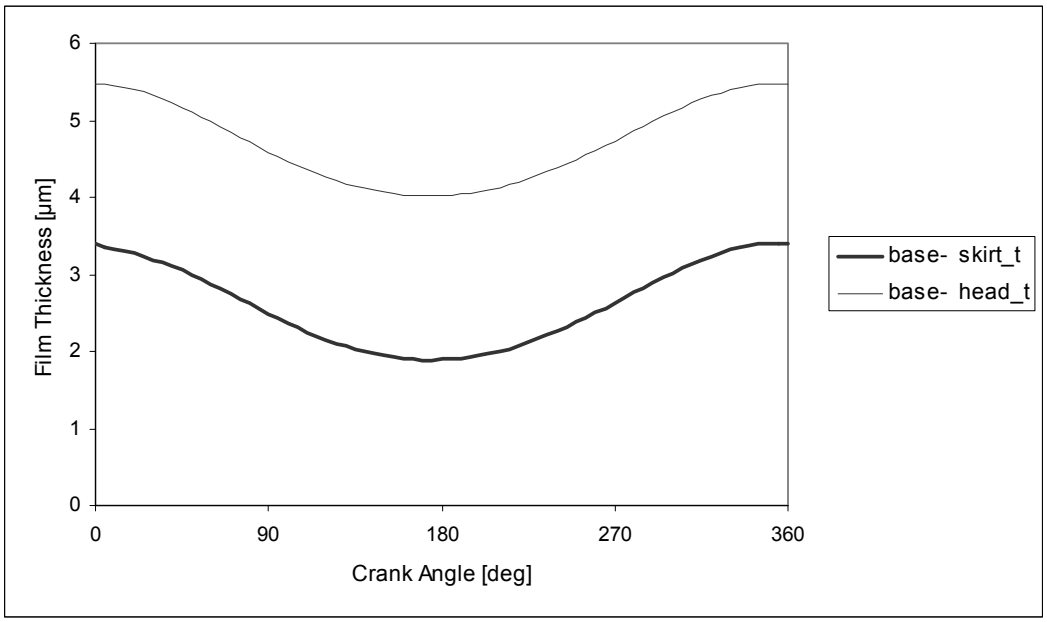

Figure 5.7 Piston thrust side skirt and head film thicknesses

In both Figure 5.7 and Figure 5.8 the difference between skirt and head film thicknesses is almost constant. This is the result of very small variation of the piston tilt angle shown in Figure 5.4.

The piston works with positive eccentricity so the anti thrust side film thicknesses are smaller. In other words, the pistons work in anti thrust side as shown in Figure 5.5.

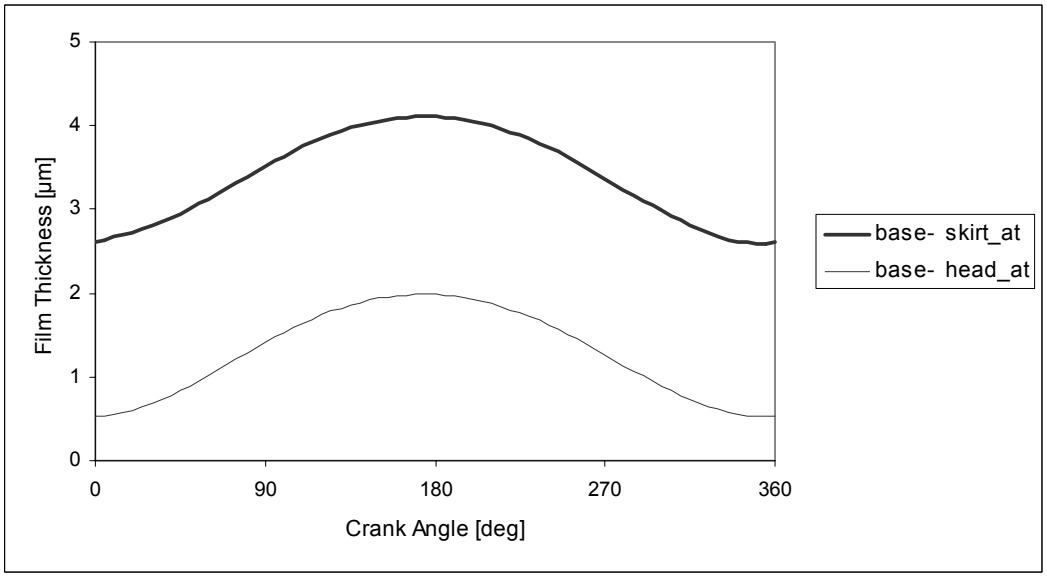

Figure 5.8 Piston anti thrust side skirt and head film thicknesses

It can be easily observed that the minimum film thickness plot in Figure 5.6 is the head anti thrust side film thickness except for the crank angles about 150˚-200˚ where head thrust side film thickness is thinner than head anti thrust side. The minimum value of the film thickness plot is at around zero degree crank angle which is very close to crank angle of maximum side load.

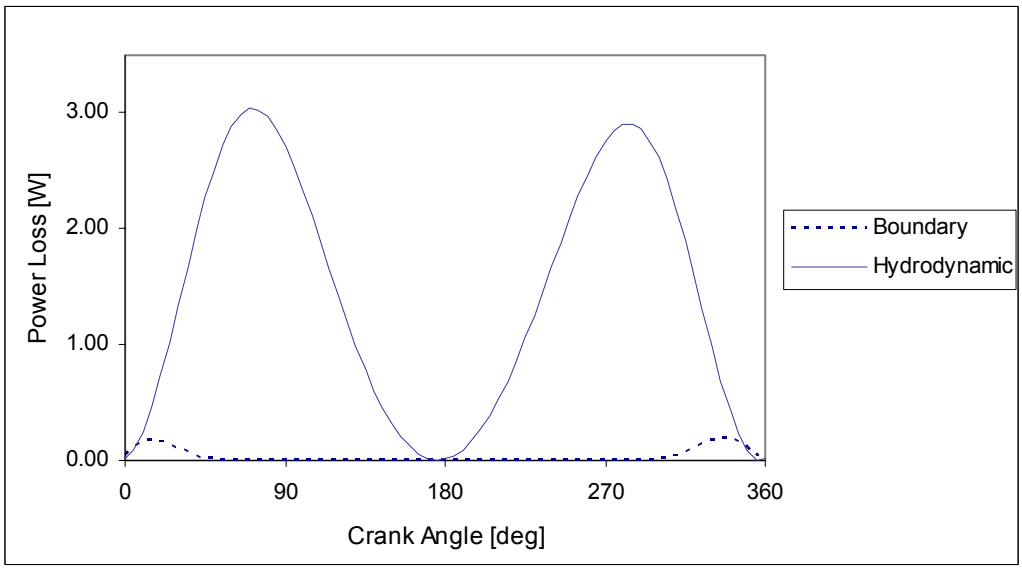

Figure 5.9 Hydrodynamic and boundary power losses

The power loss is proportional to piston speed so its sinusoidal characteristic is observed in Figure 5.9. The total cyclic power loss is calculated as 2.87 W of hydrodynamic power loss and 0.06 W of boundary power loss. As a result of the boundary contact 4.05×10^{-14} m^3/s wear rate is calculated. The boundary power lose is the result of the boundary contact of piston head anti thrust side and cylinder wall between crank angles about 315˚- 45˚. Power loss and wear rates calculated do not give the absolute values of the real case, but are useful for the comparison of different designs.

5.2.1 Single Patch Solution of the Base Model

In Section 5.2 the base model solution is given for the double patch solution areas that are illustrated in Figure 3.4 and Figure 3.5 in which DP stands for double

patch and SP stands for single patch cases. Single patch solution area shown in Figure 3.5 is used to solve again the base piston model problem to compare and understand the difference of the two approaches.

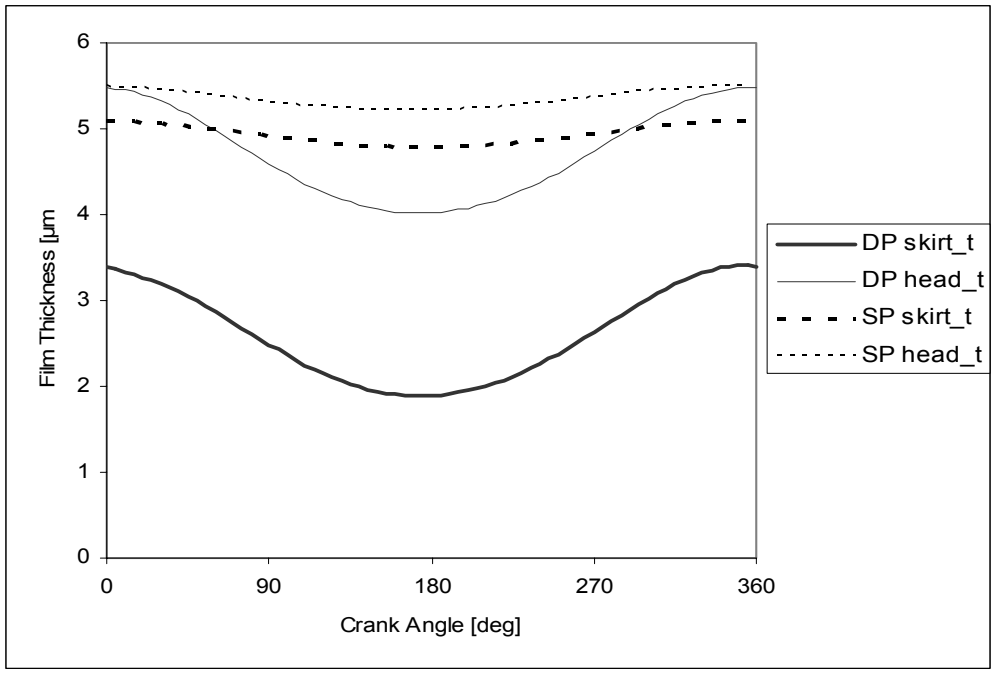

Figure 5.10 Piston thrust side skirt and head film thicknesses for single patch and double patch solutions

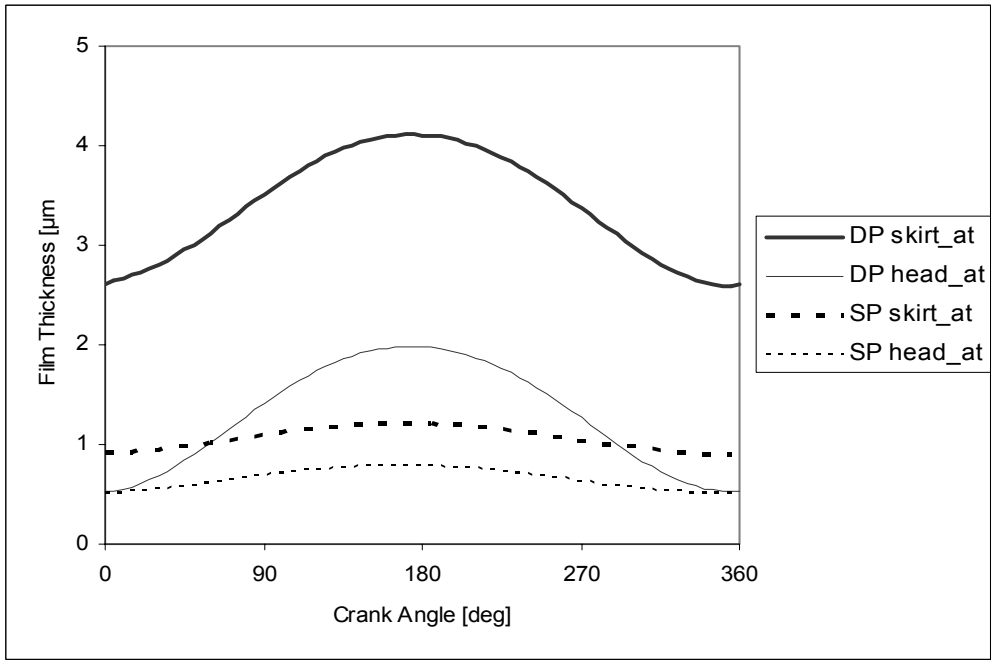

Figure 5.11 Piston anti thrust side skirt and head film thicknesses for single patch and double patch solutions

In Figure 5.10 and Figure 5.11 film thicknesses of thrust and anti thrust sides of the base piston model are shown for both double patch and single patch solutions. Two approaches predict quite different solutions for the same base piston model. According to the single patch approach the piston works at anti thrust side with positive eccentricity and very small positive tilt angle. It is easily observed that the single patch solution predicts less movement with respect to double patch solution. This is the result of the wider lubricated area which causes formation of higher oil film forces. These higher oil film forces holds piston almost at same position during the whole cycle. The piston is more eccentric to anti thrust side since lubrication dynamics of higher oil film forces pushes piston much to anti thrust side.

The double patch approach is closer to real lubrication condition of the piston. Since the wristpin hole shown in Figure 1.3 and pin assembly slot illustrated in Figure 1.4 cause a decrease in the lubricated region of the piston top and bottom sides. Hence one can assume that there is no lubrication in this area. So this not lubricated region divides the solution area two parts. As a result the double patch approach described in section 3.1 can be used.

5.3 Parametric Study

A parametric study is carried to investigate the effect of roughness (average Reynolds' equation solution), viscosity, wristpin position, groove application, groove location and groove width. During the parametric study it is important to hold all parameters used for the calculations other than the studied one constant for a correct comparative study.

The study is done only with the double patch approach described in Section 3.1 since in previous section it was concluded that double patch solution simulates the existing lubrication conditions of the compressor piston better.

5.3.1 Effect of Average Reynolds' Equation

The average Reynolds' equation's effect is expected to be significant when the clearance is relatively small with respect to surface roughness. The base piston model is solved using the average Reynolds' equation and the results are compared with the standard solution of previous section in Figures 5.12 and Figure 5.13.

The results of standard and average solutions are close to each other for base piston model. For thrust side the average model predicts thinner film thickness than standard solution. However for the anti thrust side standard solution, film thickness is thinner. Since the standard solution film thickness is lower in thrust side than anti thrust side, standard solution predicts more critical operating conditions. The average Reynolds' equation study is continued together with the viscosity study in next section.

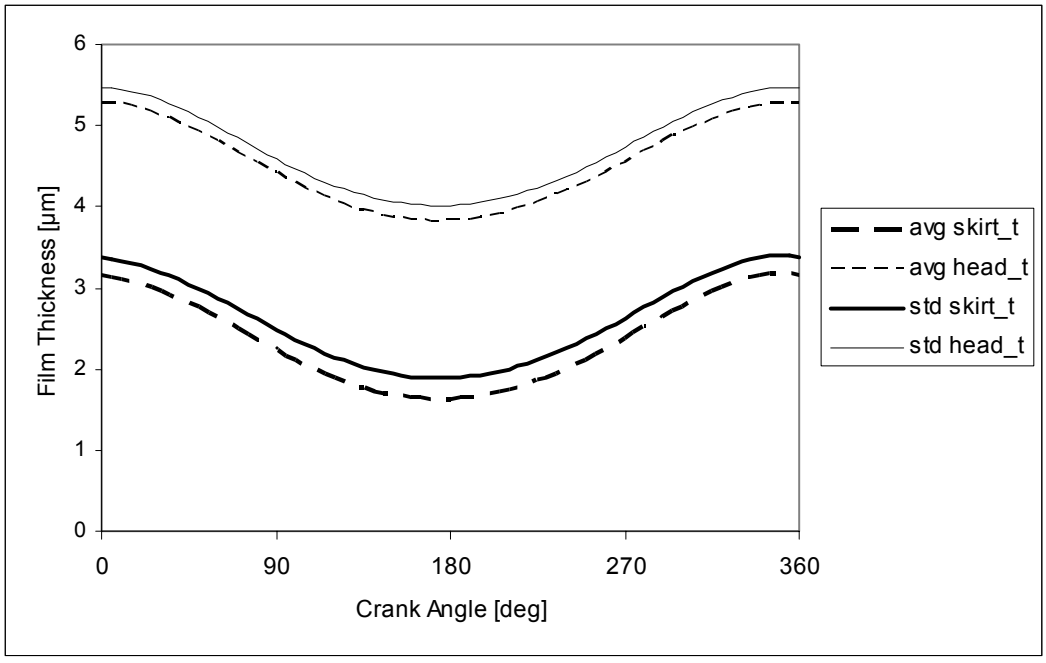

Figure 5.12 Piston thrust side skirt and head film thicknesses for standard and average solutions

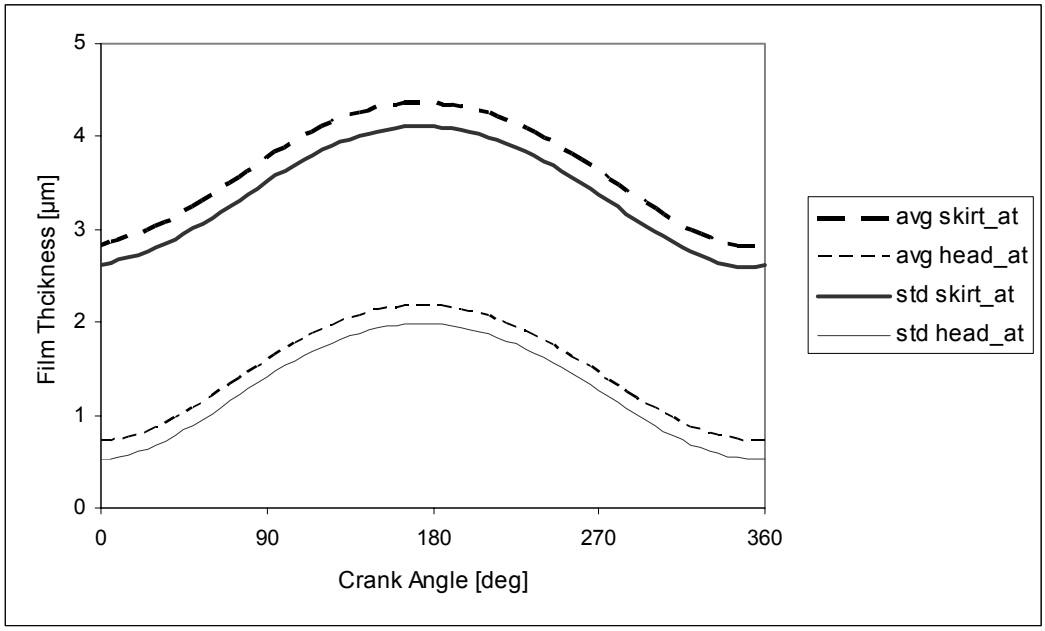

Figure 5.13 Piston anti thrust side skirt and head film thicknesses for standard and average solutions

5.3.2 Effect of Viscosity

The variation of viscosity is studied and compared with the base model. The base model viscosity is taken as 0.002 Pa.s for a 10 cSt oil under operating conditions of about 70˚C mean oil temperature. The results are plotted in Figure 5.14, Figure 5.15 and Figure 5.16 for piston eccentricity, piston tilt and minimum film thickness respectively. The symbols v3, v4, v6, v8, v10, v20 stand for 0.003 Pa.s, 0.004 Pa.s, 0.006 Pa.s, 0.008 Pa.s, 0.010 Pa.s, 0.020 Pa.s kinematic viscosity values respectively. Application of higher than 0.006 Pa.s viscosity oil is not common but in order to understand the effect, these values are selected for the study.

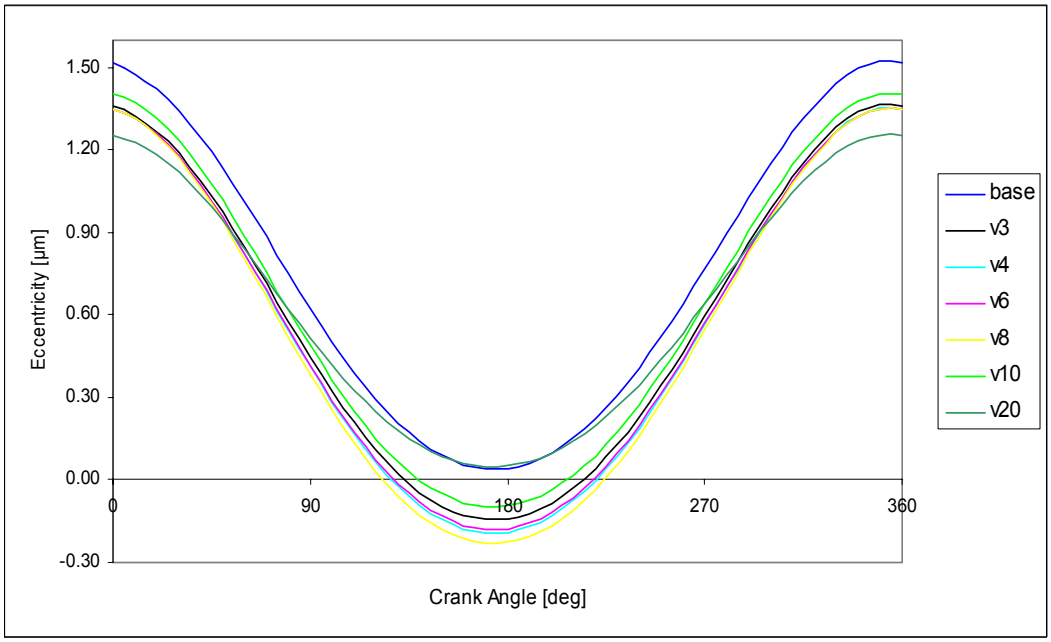

Figure 5.14 Piston eccentricities for different oil viscosities

The eccentricity in Figure 5.14 is decreasing with increasing viscosity until 0.008 Pa.s lubricant viscosity. Then the eccentricity starts decreasing with increasing viscosity.

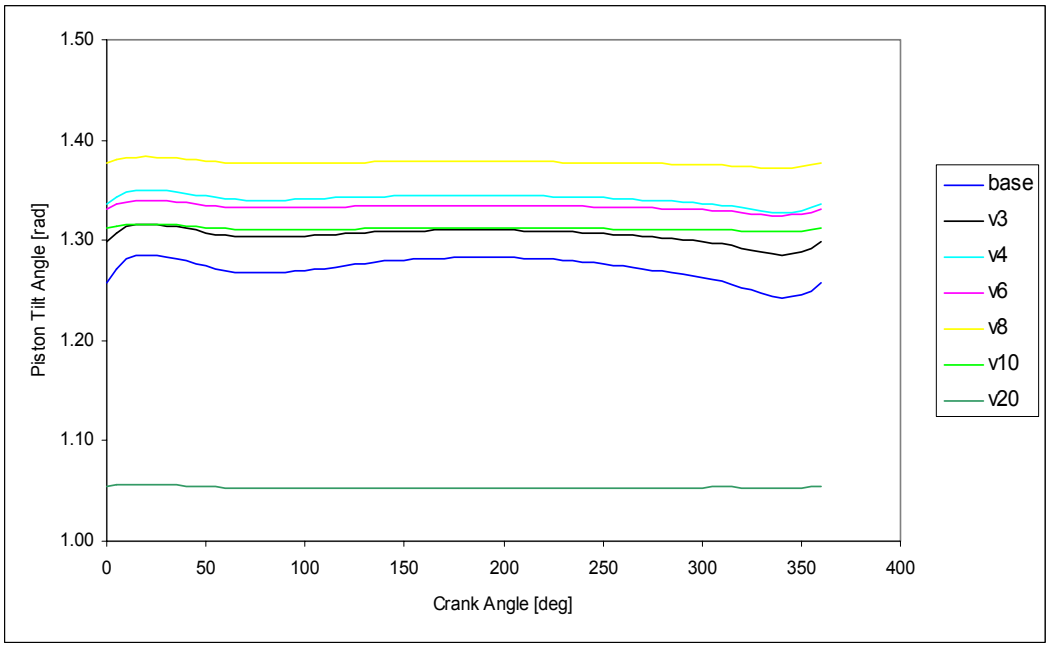

Figure 5.15 Piston tilt angle for different oil kinematic viscosities

The tilt angle in Figure 5.15 is increasing with increasing viscosity until 0.008 Pa.s. Then exceeding 0.008, the tilt angle starts decreasing with respect to 0.008 Pa.s however is still higher than for the base viscosity. But still in all cases the variation of tilt angle is very small.

In Figure 5.16 the variation of minimum film thickness plots for selected viscosity values is given. The difference among different viscosities is very small, but increasing the viscosity increases minimum film thickness at critical crank angles with respect to base 0.002 Pa.s viscosity. A significant increase is observed for 0.020 Pa.s which is a drastic viscosity increase. The interesting result is that the piston minimum film thickness is lower for 0.006 Pa.s, 0.008 Pa.s, 0.010 Pa.s than 0.003 Pa.s viscosity however the difference is almost negligible.

When the eccentricity decreases with increasing viscosity tilt angle increases, and when eccentricity starts increasing tilt angle starts decreasing. The decrease in eccentricity increases the minimum film thickness at the critical crank angles where film thickness of head anti thrust side given in Figure 5.18 is below 1µm.

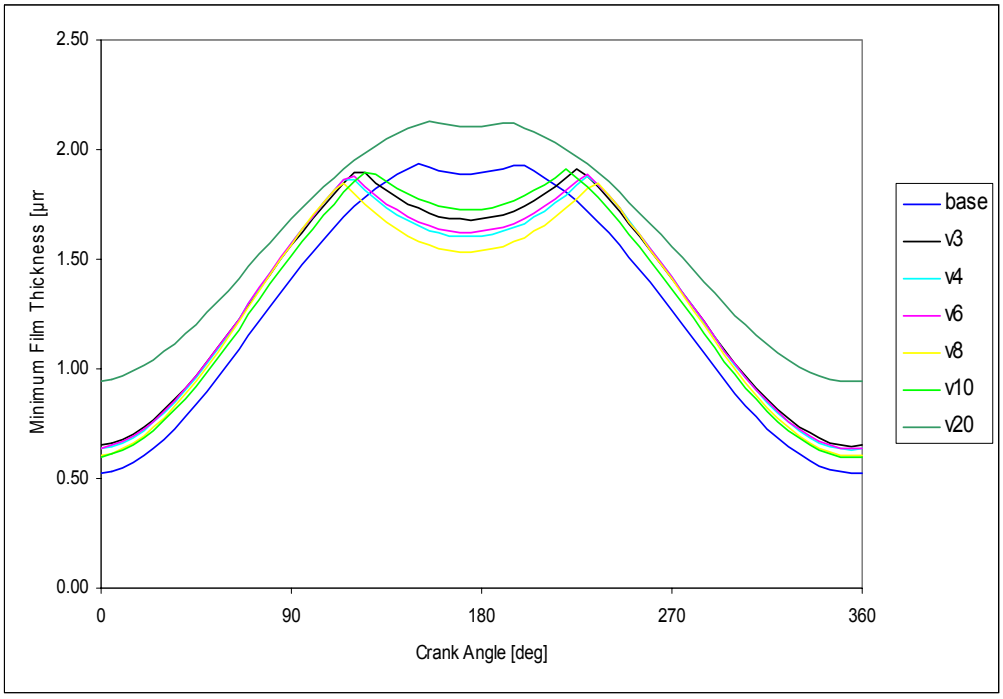

Figure 5.16 Minimum film thickness plots for different viscosity values

Similar trend in eccentricity variation for increasing viscosity is present for the film thickness plots given in Figure 5.17 and Figure 5.18.

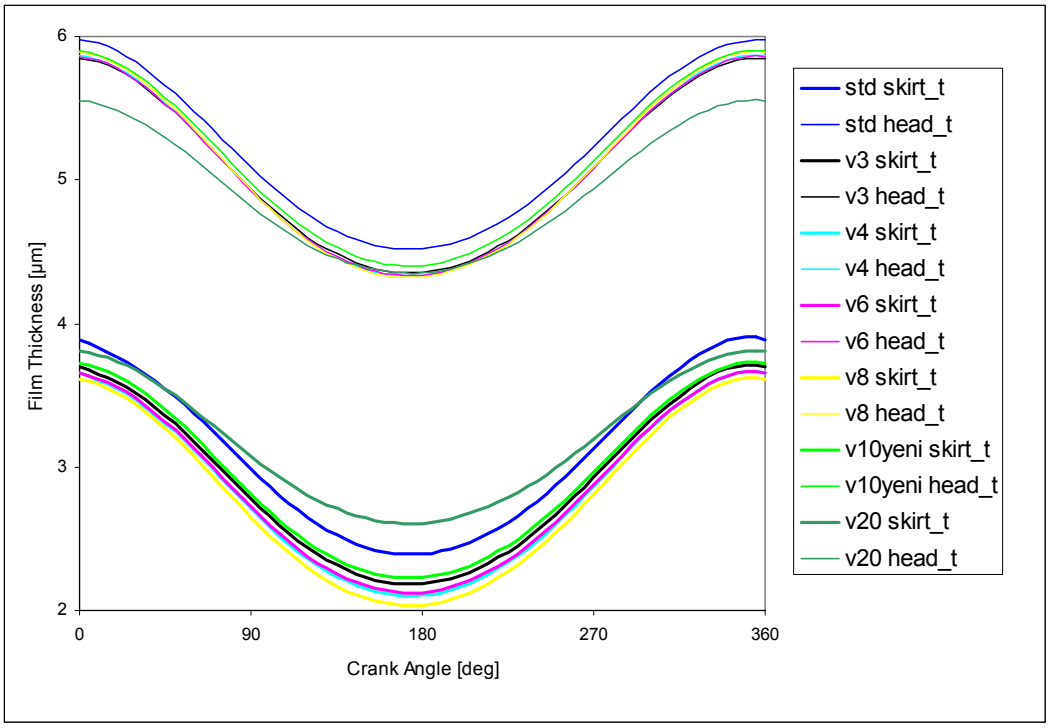

Figure 5.17 Piston thrust side skirt and head film thicknesses for different oil viscosities

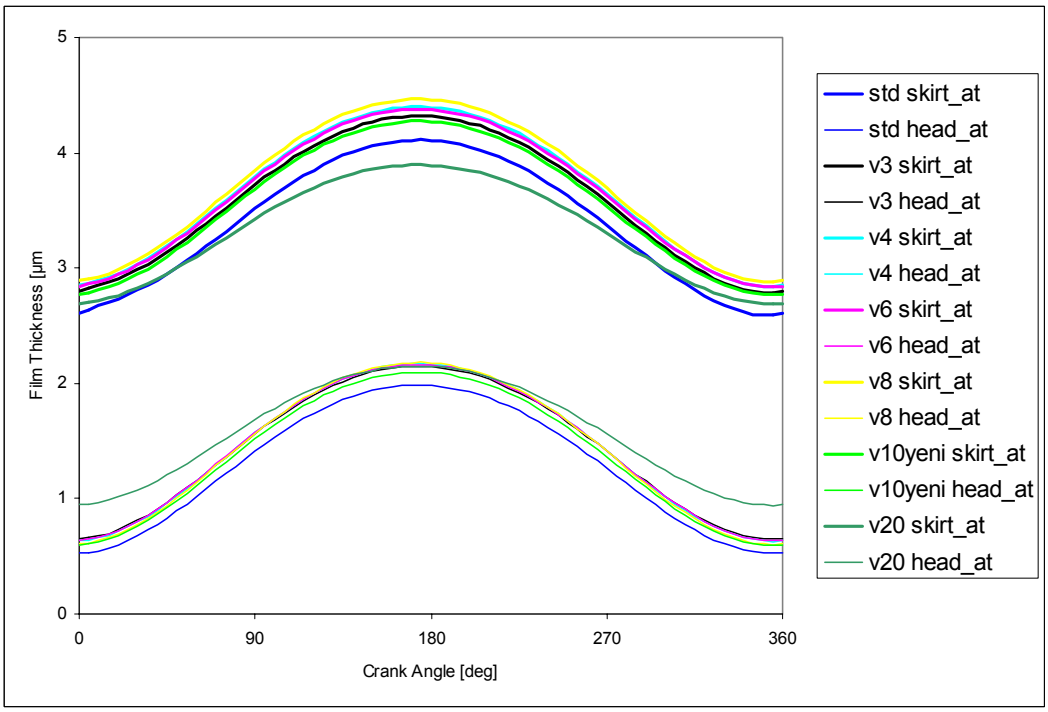

Figure 5.18 Piston anti thrust side skirt and head film thicknesses for different oil viscosities

As given in Table 5.1 hydrodynamic power loss is increasing with increasing viscosity as usual. However because of increasing eccentricity of the piston with increasing viscosity the boundary loss slightly increases causing a slight increase in wear rate.

Table 5.1 Power loss and wear rate values for different kinematic viscosity values

case	*Power Loss [W]*		*Wear Rate [m3/s]*
	Hydrodynamic	*Boundary*	
base	2.87	0.06	4.05E-14
v3	4.31	0.07	4.27E-14
v4	5.75	0.08	4.87E-14
v6	8.62	0.07	4.62E-14
v8	11.52	0.10	6.10E-14
10	13.59	0.00	0.00E+00
v20	28.18	0.00	2.15E-15

When the viscosity is extremely low, the standard solution predicts smaller film thickness values, so one can conclude that standard solution can be used for safe design. In the following graphics v1 stands for 0.001 Pa.s kinematic oil viscosity. In Figure 5.19 the head thrust side film thickness of standard solution is extremely low resulting in boundary lubrication.

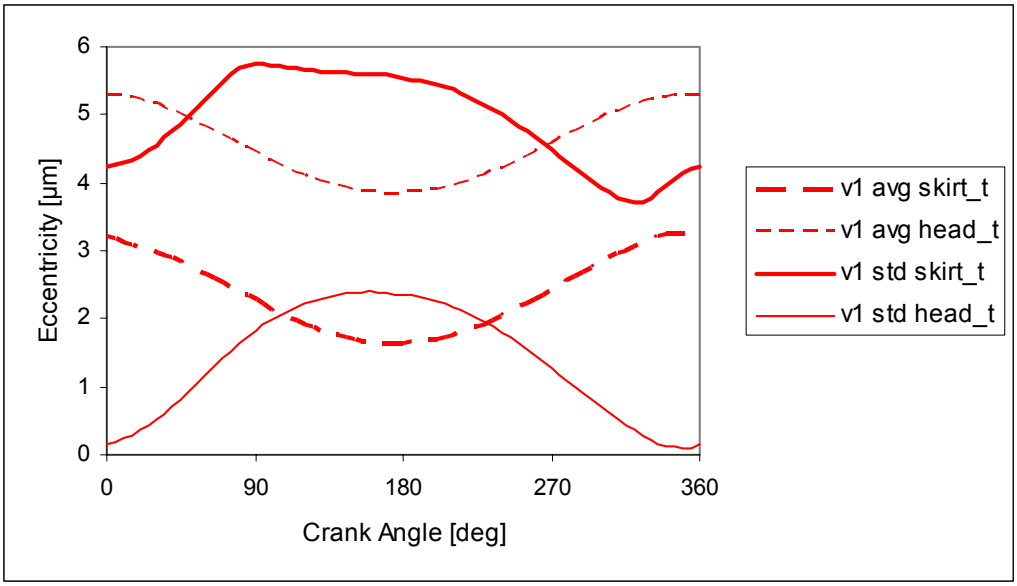

Figure 5.19 Piston thrust side skirt and head film thicknesses of average and standard solutions for 0.001 Pa.s oil viscosities

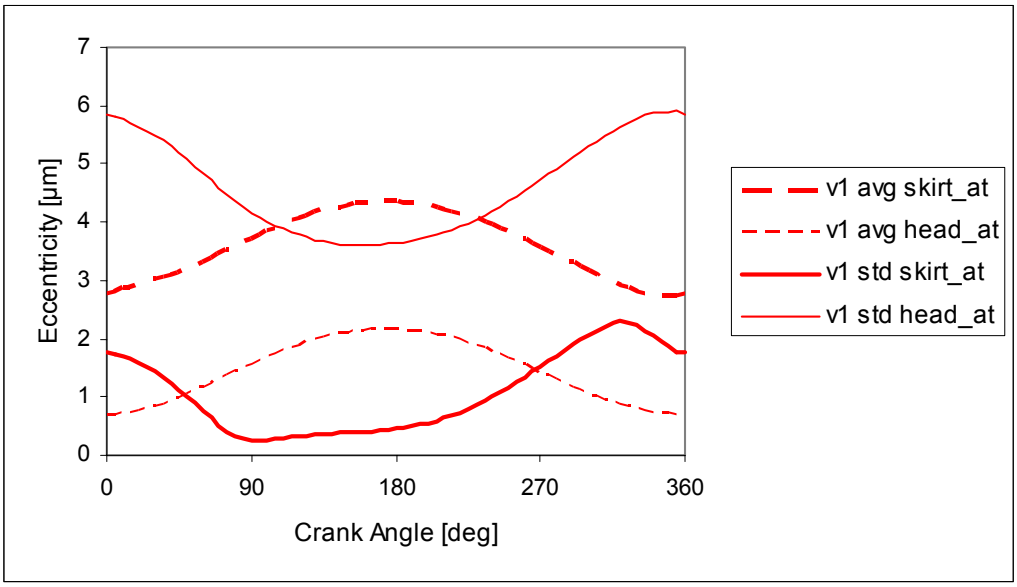

Figure 5.20 Piston anti thrust side skirt and head film thicknesses of average and standard solutions for 0.001 Pa.s oil viscosities

As result of the severe working conditions predicted by the standard solution, the boundary power loss is calculated as 4.92 W as shown in Table 5.2. However it is calculated as 0.05 W by the average solution. And there is almost 2 orders of difference between wear rates.

Table 5.2 Power loss and wear rate values of 0.001 Pa.s viscosity for average and standard Reynolds' equation solutions

case	*Power Loss [W]*		*Wear Rate [m3/s]*
	Hydrodynamic	*Boundary*	
v1 std	1.62	4.92	2.18E-12
v1 avg	1.33	0.05	2.82E-14

Film thickness plots of standard solution and average solutions are given in appendix-A for all viscosity values except 0.001 Pa.s that are given in Figure 5.19 and Figure 5.20. The figures show that the film thickness variations are similar. And it is clear that standard solution always predicts more critical operating conditions for the selected roughness characteristic as a result of thinner oil film formations at head anti thrust sides.

5.3.3 Effect of Wristpin Location

The position of wristpin is changed in axial z-direction to investigate the effect of its location with respect to center of mass. Changing the wristpin location affects the equation of motion since the moment of the force of connecting rod on piston, around piston center of mass changes.

The wristpin location of the base model is at 6.665 mm from piston skirt and piston center of mass is at 8.965 mm from piston skirt. So the wristpin location is 2.3 mm away to skirt side from piston center of mass.

The solutions are given only for standard solution of Reynolds' equation because this solution predicts more critical operating conditions. In the Figure 5.21 and Figure 5.22 the results of film thicknesses of the cases that the wristpin position is moved to center of mass, moved 2 mm to skirt side (4.3 mm away from center of mass) and 4.3 mm to head side (2 mm away from center of mass to head side) are given together with the base piston model.

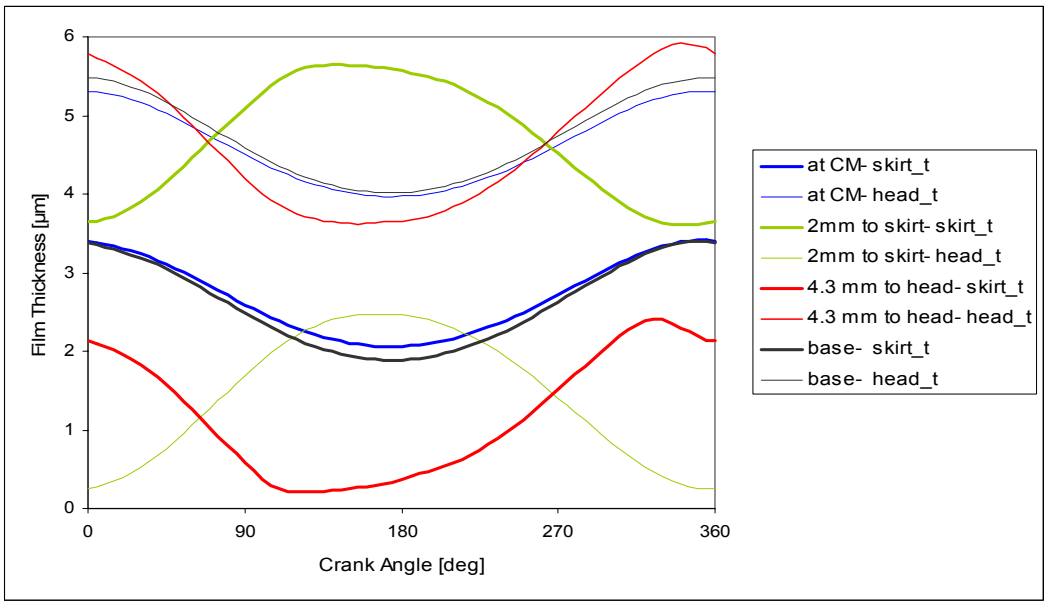

Figure 5.21 Piston thrust side skirt and head film thicknesses for different wristpin positions

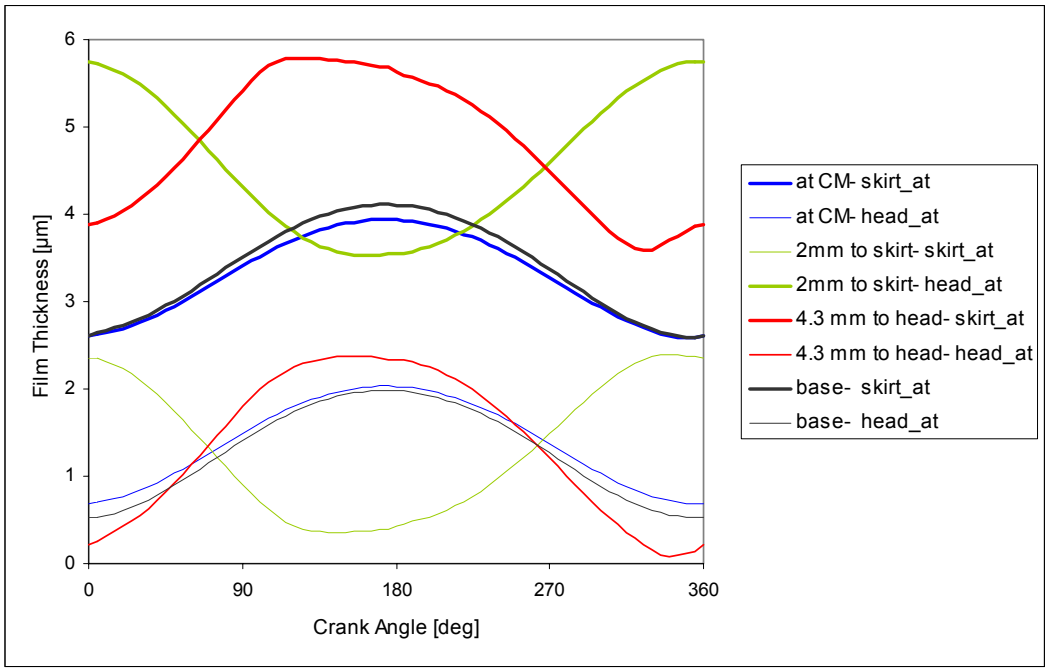

Figure 5.22 Piston anti thrust side skirt and head film thicknesses for different wristpin positions

From the results it can be concluded that wristpin position at center of mass or close to center of mass is better for piston lubrication. Since the higher film thickness for head anti thrust side is the case with wristpin at center of mass.

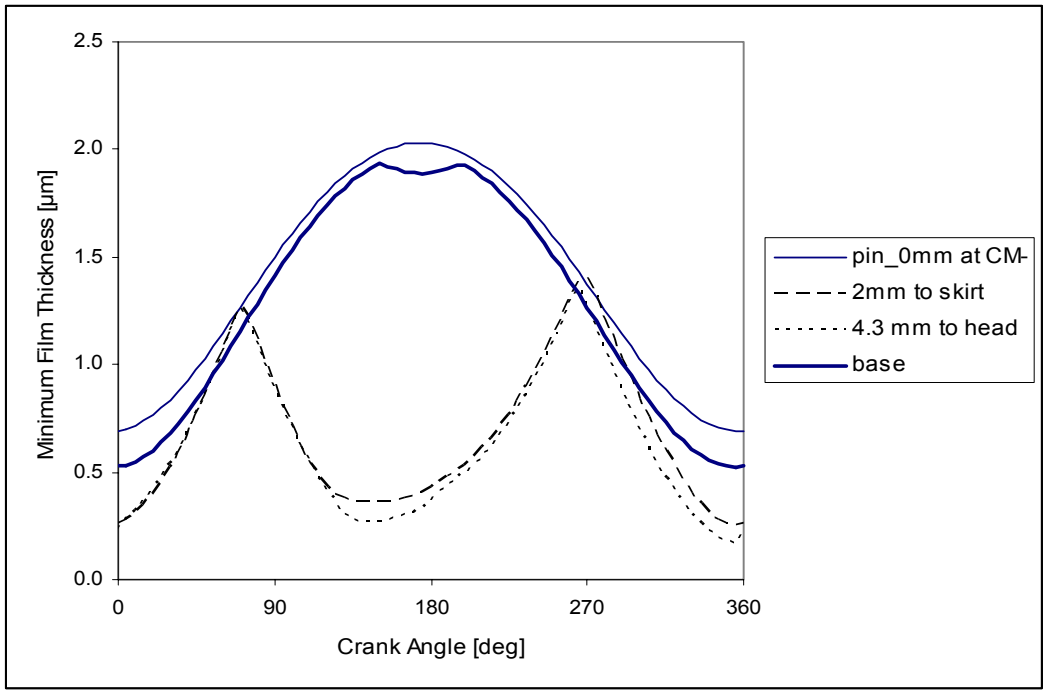

Figure 5.23 Minimum film thickness plots for different wristpin locations

In the minimum film thickness graphics wristpin at center of mass has the highest film thickness values and 2 mm to skirt case follows it with similar minimum film thickness plot that are given in Figure 5.23. Moving the wristpin position far from center of mass is disadvantageous since it causes a thinner oil film and increases boundary power loss together with wear rate. Results are given in Table 5.3.

Table 5.3 Power loss and wear rates for pistons with different wristpin locations

case	*Power Loss [W]*		*Wear Rate [m3/s]*
	Hydrodynamic	*Boundary*	
at CM	2.90	0.05	3.27E-14
2mm to skirt	3.07	1.72	1.07E-12
4.3 mm to head	2.73	2.61	1.61E-12
base	2.87	0.06	4.05E-14

5.3.4 Effect of Groove

The effect of groove is studied by changing groove location and groove width. First the effect of groove existence is investigated. A piston model with no groove is named as no groove in Figure 5.24, Figure 5.25 and Figure 5.26 and compared with the base piston model with groove.

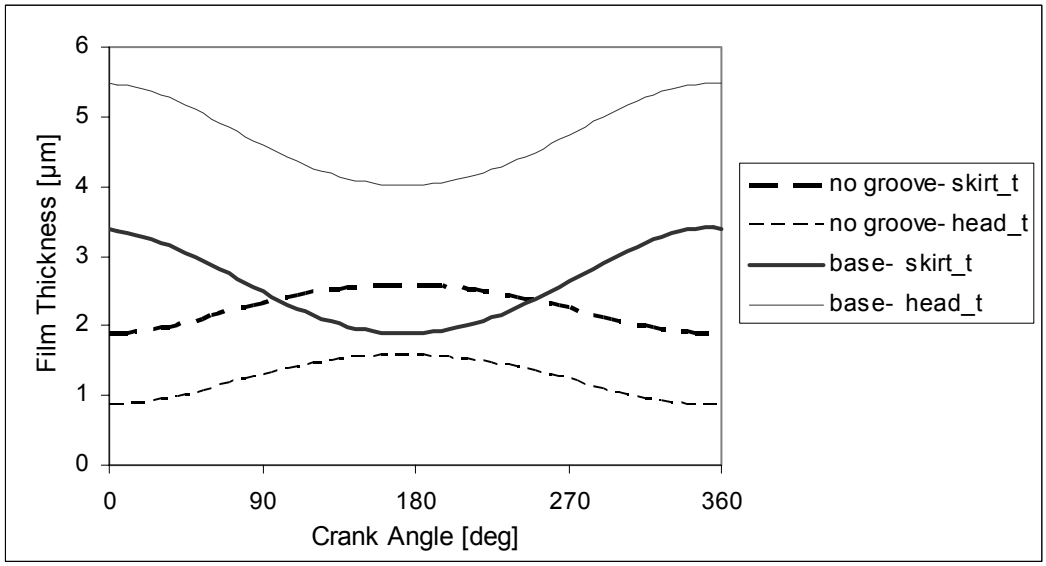

Figure 5.24 Piston thrust side skirt and head film thicknesses for pistons with groove and without groove

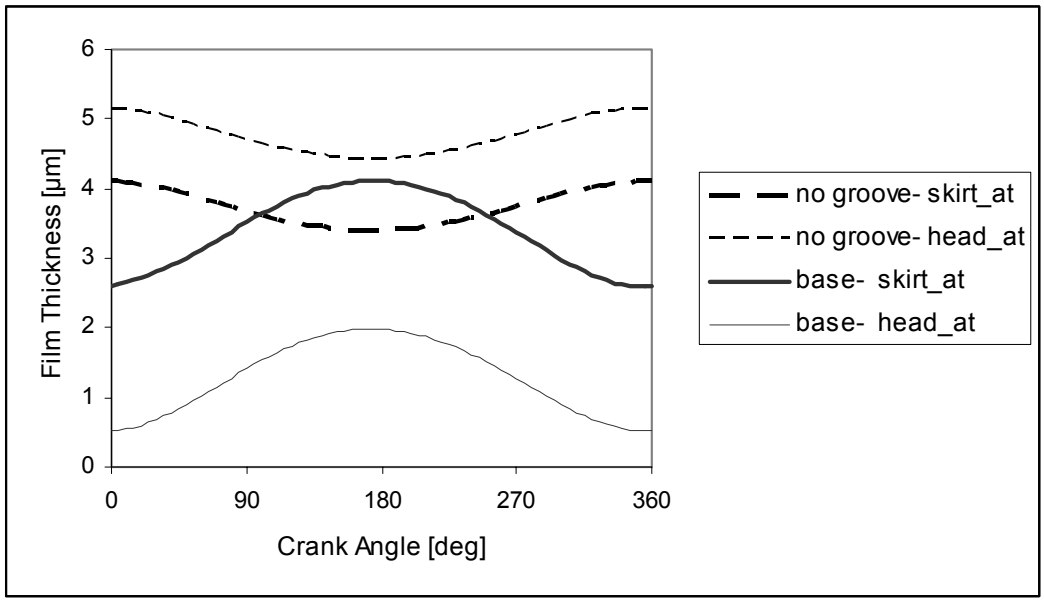

Figure 5.25 Piston anti thrust side skirt and head film thicknesses for pistons with groove and without groove

A commentary on Figure 5.24 and Figure 5.25 shows that the piston without groove works with negative tilt angle at thrust side. The tilt angle of piston without groove is smaller in magnitude than the base piston model with groove, and also eccentricity variation is smaller. As the lubricated area of the piston without groove is larger, oil film pressures are lower. So smaller squeezing eccentric movements, and smaller tilt angle of the wedge effect are sufficient. As a result, minimum film thickness given in Figure 5.26 is thicker between crank angles about 280˚ – 80˚ for the piston without groove.

The primary motivation for using a groove is to reduce the sliding bearing area hence to reduce the power loss because of the reduction of hydrodynamic losses. On the other hand possible increase in the boundary power loss must stay in an acceptable range which is the designer's decision. In table 5.4 as expected there is 1 W decrease in hydrodynamic losses beside 0.03 W increase in boundary losses by the application of groove. There is slight increase in wear as a result of higher boundary forces. So from power loss point of view using a piston with groove is advantageous.

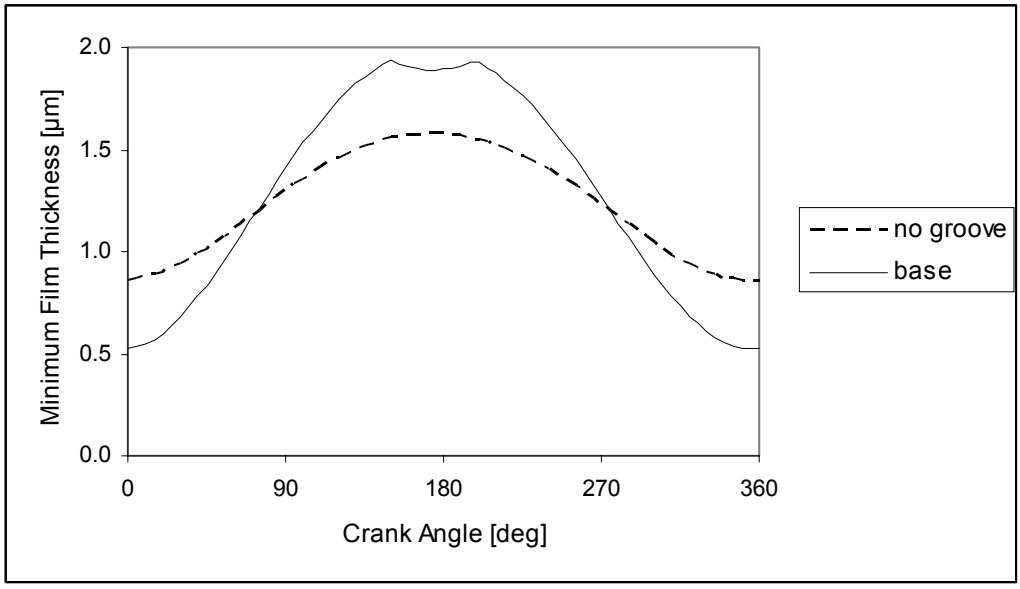

Figure 5.26 Minimum film thickness plots for pistons with groove and without groove

Table 5.4 Power loss and wear rates for pistons with and without groove

case	*Power Loss [W]*		*Wear Rate [m3/s]*
	Hydrodynamic	*Boundary*	
no groove	3.82	0.03	1.28E-14
base	2.87	0.06	4.05E-14

Secondly, the groove location is changed in both head and skirt directions. First the results for only movement to the skirt side are compared with base model in which the groove is moved 2 mm and 4 mm from its base position. Groove of the base piston model is 2.82 mm wide and starts at 7.04 mm away from skirt side.

Figure 5.27 and Figure 5.28 show the film thickness values for the different groove locations and the results are compared with the base model. Both 2 mm and 4 mm location change sign of piston tilt angle. In these cases piston tilt is negative. And for 2 mm tilt angle's magnitude is significantly increasing. The film thickness of head thrust side drops below 1 µm about 0˚ crank angle. But for the anti thrust side film thickness is higher about 0˚ crank where the for base model film thickness is about 0.5 µm. On the other hand between 90˚ - 270˚ crank angles the skirt anti thrust side film thickness decreases with respect to the base model.

Hence lower minimum film thickness values are obtained between these angles resulting in higher wear rate and boundary power loss as given in Table 5.5.

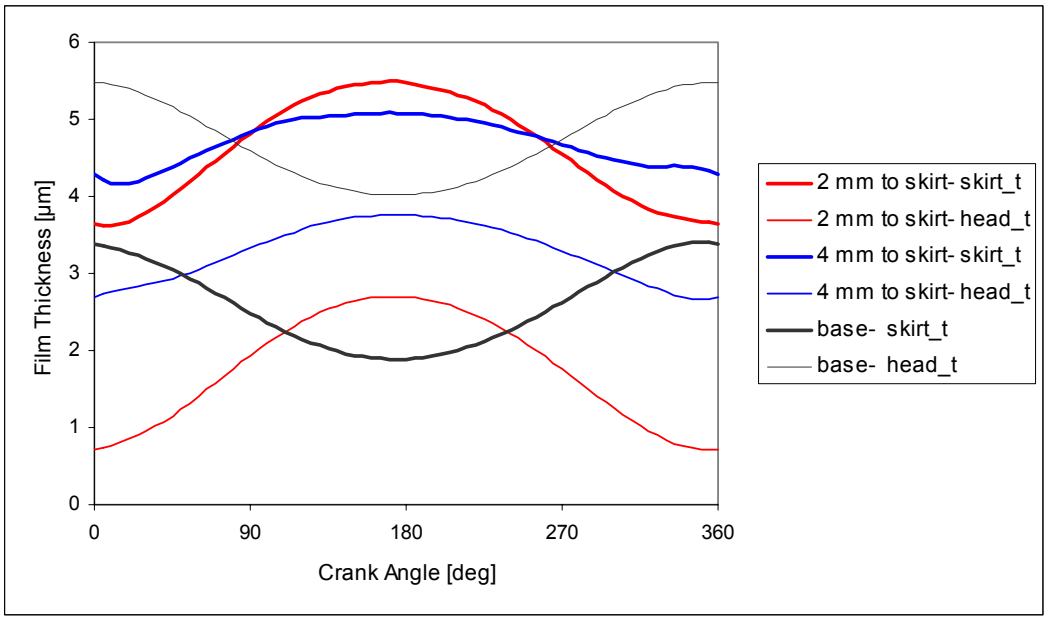

Figure 5.27 Piston thrust side skirt and head film thicknesses for pistons with grooves moved to skirt side

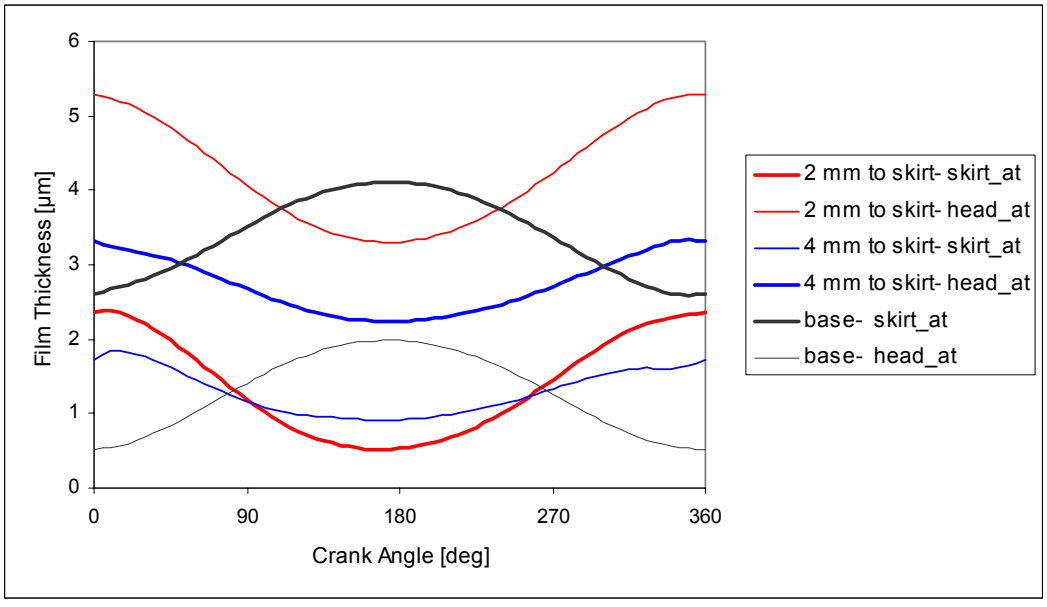

Figure 5.28 Piston anti thrust side skirt and head film thicknesses for pistons with grooves moved to skirt side

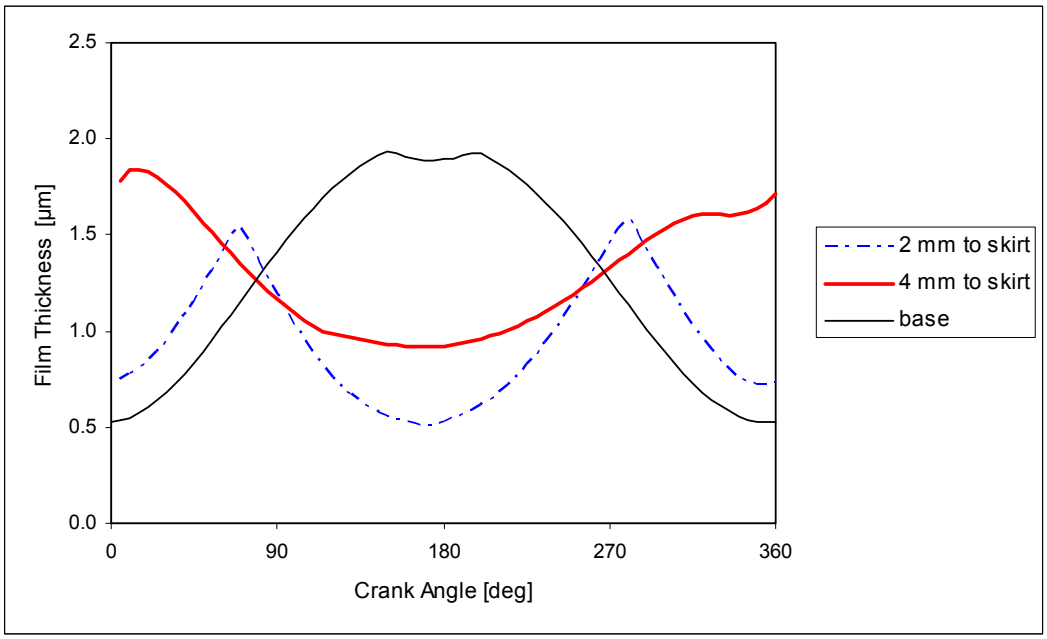

Figure 5.29 Minimum film thickness plot for pistons with grooves moved to skirt side

Table 5.5 Power loss and wear rates for pistons with grooves moved to skirt side

case	*Power Loss [W]*		*Wear Rate [m3/s]*
	Hydrodynamic	*Boundary*	
2 mm to skirt	2.91	0.19	1.49E-13
4 mm to skirt	2.88	0.01	6.05E-15
base	2.87	0.06	4.05E-14

Moving the groove 4 mm decreases boundary power loss and wear rate since there is a significant increase in minimum film thickness for crank angles 270˚ - 360˚. The minimum film thickness is lower than the base model between 90˚ - 270˚ but it is not lower than 1 µm on the other hand minimum film thickness is almost 0.5 µm at 0˚ (360˚) crank angle (Figure 5.29). So at overall cycle the film thickness does not fall below 1 µm for 4 mm groove movement.

Then the groove is moved to head side, and the results are compared with base piston model in Figure 5.30, Figure 5.31 and Figure 5.32. From the skirt thrust side and head anti thrust side plots it is clear that moving the groove to head side

decreases the film thickness with respect to base piston, causing heavier working conditions. Similar conclusion can be reached form minimum film thickness plot in Figure 5.32 in which drastic decrease in minimum film thickness is observed.

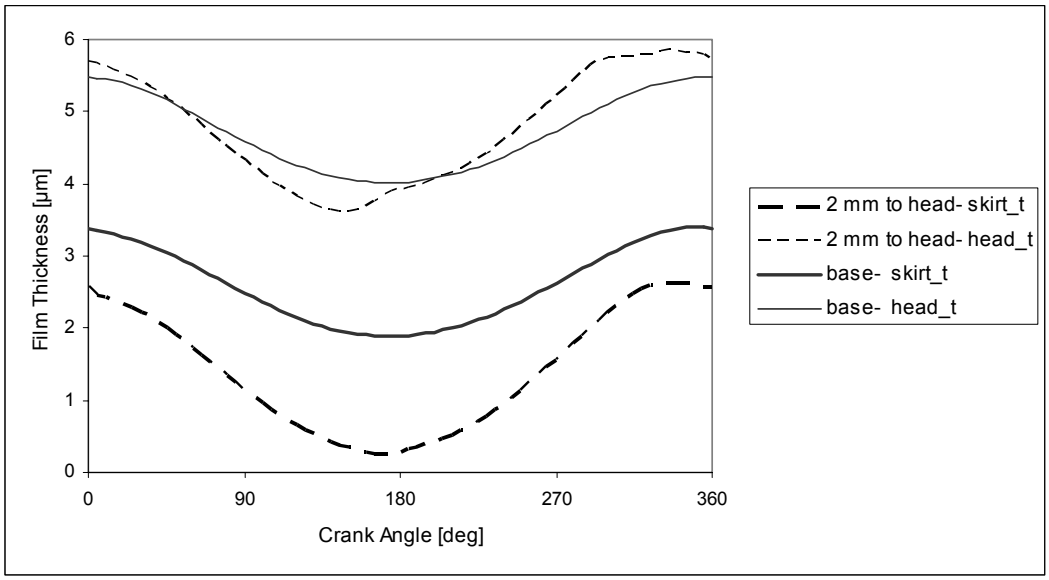

Figure 5.30 Piston thrust side skirt and head film thicknesses for piston with groove moved to head side

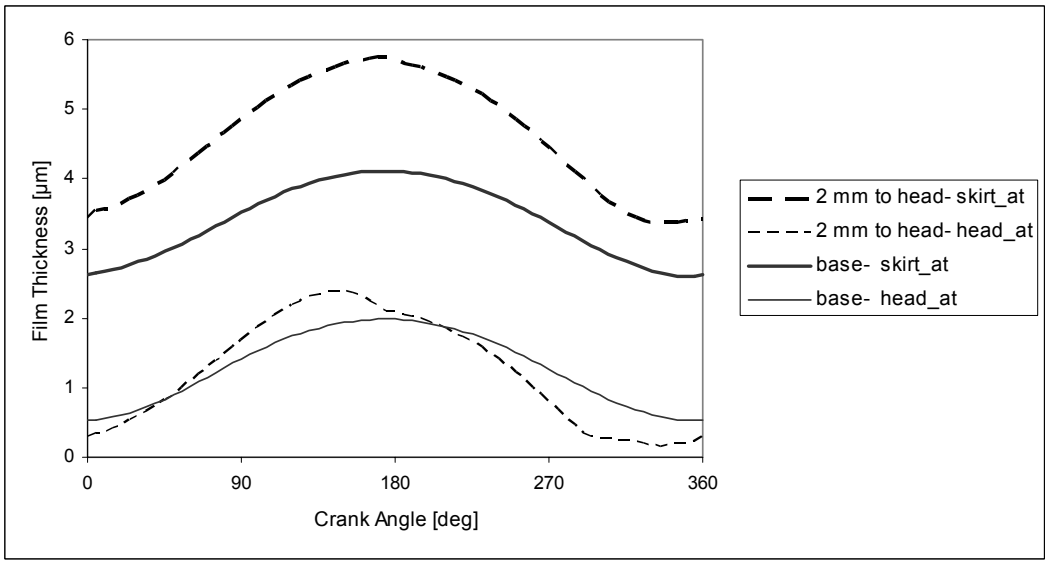

Figure 5.31 Piston anti thrust side skirt and head film thicknesses for piston with groove moved to head side

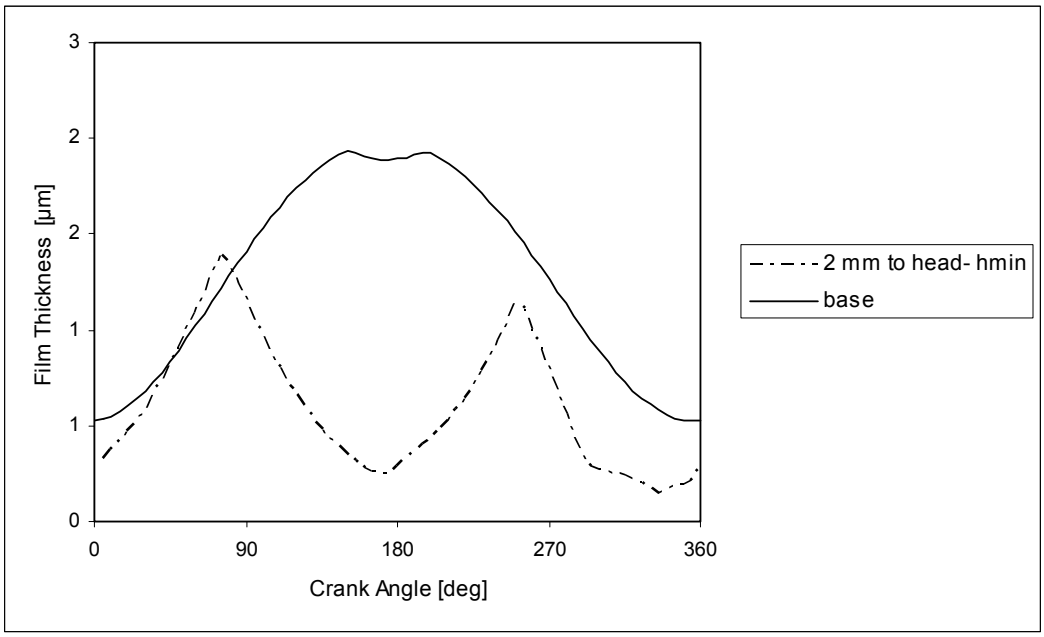

Figure 5.32 Minimum film thickness plot for pistons with grooves moved to skirt

From the power loss and wear rate results in Table 5.6 the severe working condition of the modified piston is observed. The boundary power loss increases to a higher value than the hydrodynamic loss by a 4.27 W jump with respect to the base. And there is significant increase in wear rate as result.

Table 5.6 Power loss and wear rates for piston with grooves moved to head side

case	*Power Loss [W]*		*Wear Rate [m3/s]*
	Hydrodynamic	*Boundary*	
2 mm to head	3.16	4.33	2.05E-12
base	2.87	0.06	4.05E-14

The results of groove location study verify that it is better to study the effect of groove width by extending it in skirt direction. The groove width is increased 2 mm and 4 mm to skirt side. Furthermore, the 2 mm wider groove is moved 2 mm to skirt side as an additional case. The results for skirt/head thrust/anti thrust sides' film thicknesses are given in Figure 5.33 and Figure 5.34. In the related graphics w2 stands for 2 mm wider, w4 stands for 4 mm wider groove, w2m2 stands for 2 mm wider groove that is also moved 2 mm to skirt side.

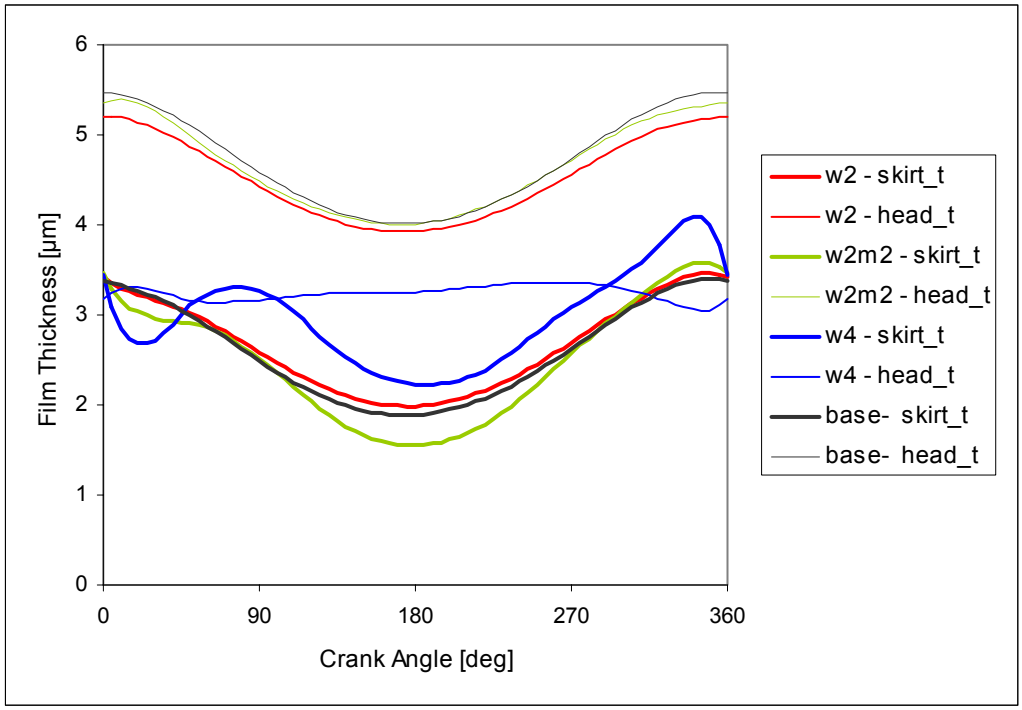

Figure 5.33 Piston thrust side skirt and head film thicknesses for piston with different groove widths

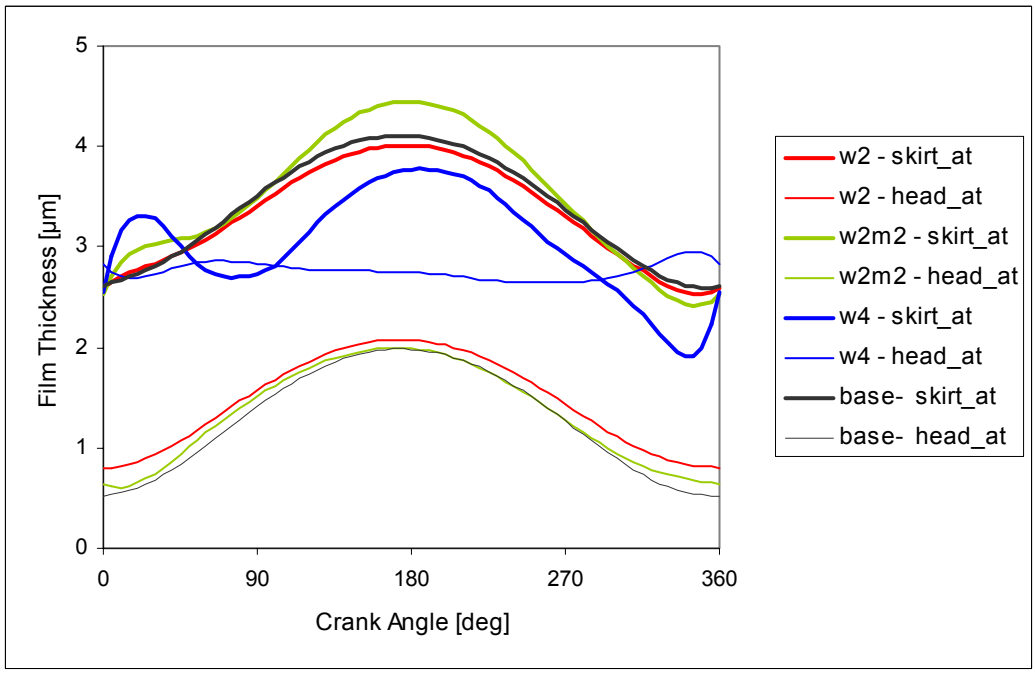

Figure 5.34 Piston anti thrust side skirt and head film thicknesses for piston with different groove widths

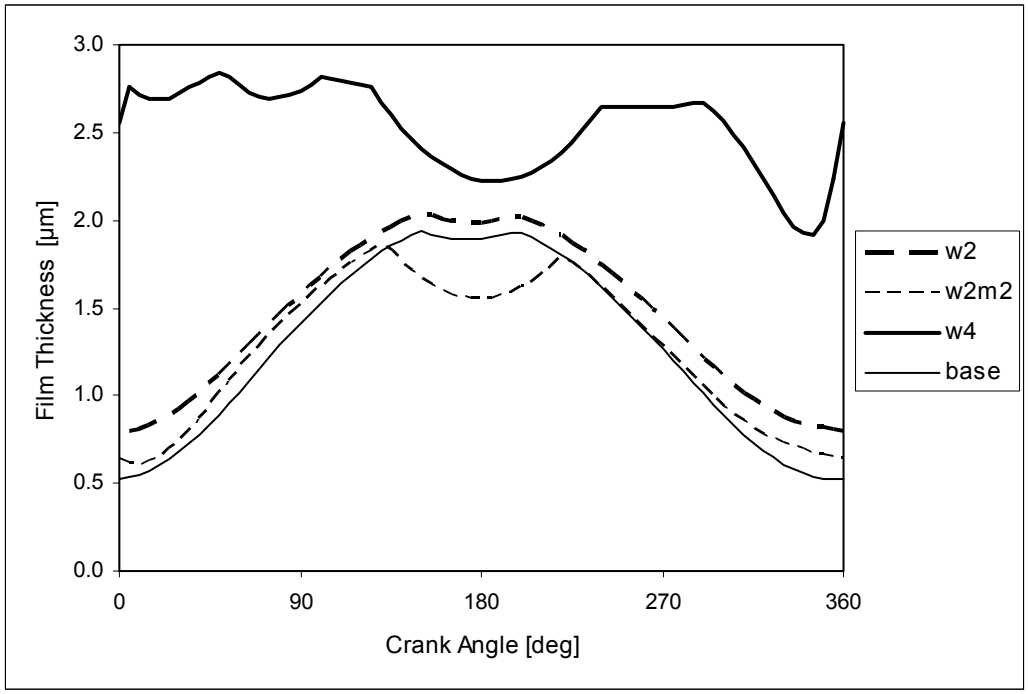

Figure 5.35 Minimum film thickness plots for pistons with different groove widths

Table 5.7 Power loss and wear rates for pistons with different groove widths

case	*Power Loss [W]*		*Wear Rate [m3/s]*
	Hydrodynamic	*Boundary*	
w2	2.46	0.02	1.14E-14
w2m2	2.53	0.10	6.00E-14
w4	1.83	0.00	0.00E+00
base	2.87	0.06	4.05E-14

For the cases that the groove is 2 mm wider (w2) and is 2 mm wider and moved 2 mm to skirt side (w2m2), the results of piston secondary dynamics are very similar to the base model. Because of the reduction in sliding bearing surface area, there is a decrease in hydrodynamic power loss (Table 5.7).

For the case of 4 mm wider groove, piston works almost at the center of the cylinder with a very small tilt angle. The film thickness around head side is almost uniform and close to 3 µm which can be observed from Figure 5.33, Figure 5.34 and minimum film thickness plot, Figure 5.35. For the skirt side there is a

variation between 2 μm and 4 μm film thickness. So the piston does not work in boundary lubrication regime and has no boundary power loss as given in Table 5.7. And as a result of wider groove, the hydrodynamic power loss decreases to 1.83 W from 2.87 W since the bearing area is reduced with increasing groove width.

CHAPTER VI

CONCLUSION

Piston design parameters; viscosity, wristpin axial location, groove location and width are studied to understand their effects on lubrication dynamics of a reciprocating compressor piston. The standard and average Reynolds' equations are solved and compared. Since the standard solution predicts more critical operating conditions for the selected bearing roughness characteristic, it is decided to do the parametric study by using it.

- From the solution and commitment of the base piston model it is seen that the piston works at thrust side with a very small tilt angle variation.
- The squeeze effect alone can create sufficient hydrodynamic oil film force to carry the piston side load.
- The minimum film thickness occurs close to 0˚ crank angle where the side load reach its maximum value.
- Comparing the double patch and single patch approaches shows that double patch assumption is closer to the real conditions of the piston since wristpin hole on the piston and pin assembly slot on the cylinder reduces the lubricated area.
- Increasing the viscosity does not significantly effects the piston secondary dynamics. Since the cylinder pressure boundary condition, alone increases the film pressure enough to carry the side load.
- Standard Reynolds' equation predicts more critical operating conditions as a result of the thinner oil film prediction for all higher kinematic viscosity values.
- Low viscosity operating conditions cause piston work in boundary lubrication regime.

- Altering the wristpin position shows that pin at center of mass or close to center of mass should be preferred since pin position far from center of mass worsens the lubrication.
- Moving the wristpin of the base piston to a location between center of mass and piston head is disadvantageous.
- Using a groove is advantageous from power loss point of view as power loss decreases with decreasing sliding area.
- Without changing the width, moving the groove of the base model to head side should be avoided since it causes very low oil film formation and boundary lubrication.
- Moving and extending the groove to skirt side decreases power loss and wear rates.
- With a groove extended 4 mm to skirt side, complete hydrodynamic lubrication conditions are achieved.

It is vital to note that all the conclusions listed are restricted with the assumptions considered when the model is developed such as rigid surfaces, neglected viscosity variations and thermal deformations due to temperature variations, neglected piston and cylinder hole circularities due to manufacturing processes etc.

The model can be improved as a future work by adding the neglected effects of surface deformations, viscosity thermal variations and surfaces' circularity characteristics. A dynamic solution area can be used to model the case in which some portion of piston skirt goes out the cylinder hole during operation when piston goes to the bottom dead center. Also finite volume approach can be used instead of finite difference approach for the numeric solution of Reynolds' equation to simulate the oil flows in the piston-cylinder bearing.

APPENDIX A

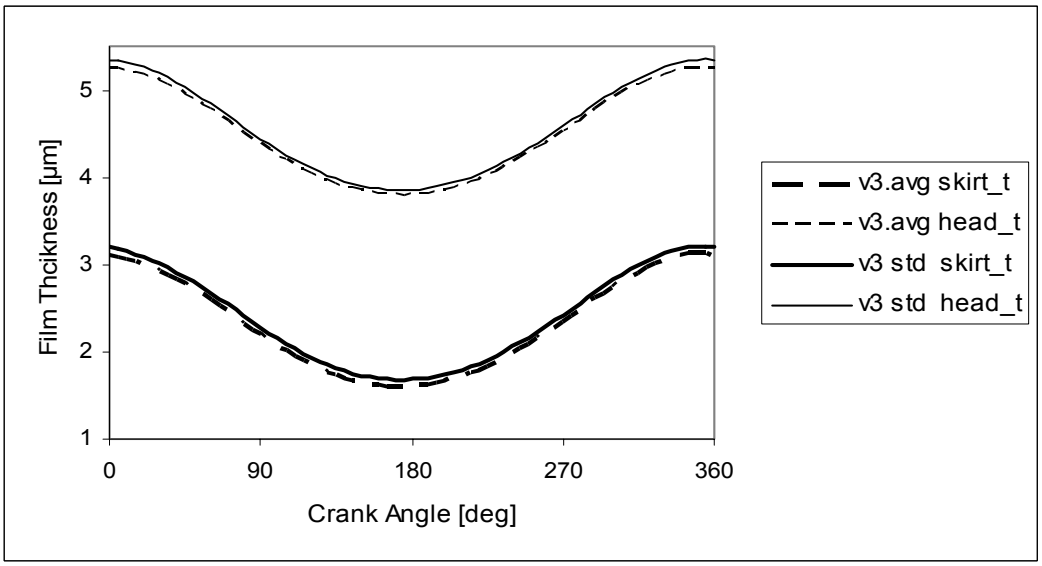

Figure A.1 Piston thrust side skirt and head film thicknesses of standard and average solutions for 0.003 Pa.s oil kinematic viscosity

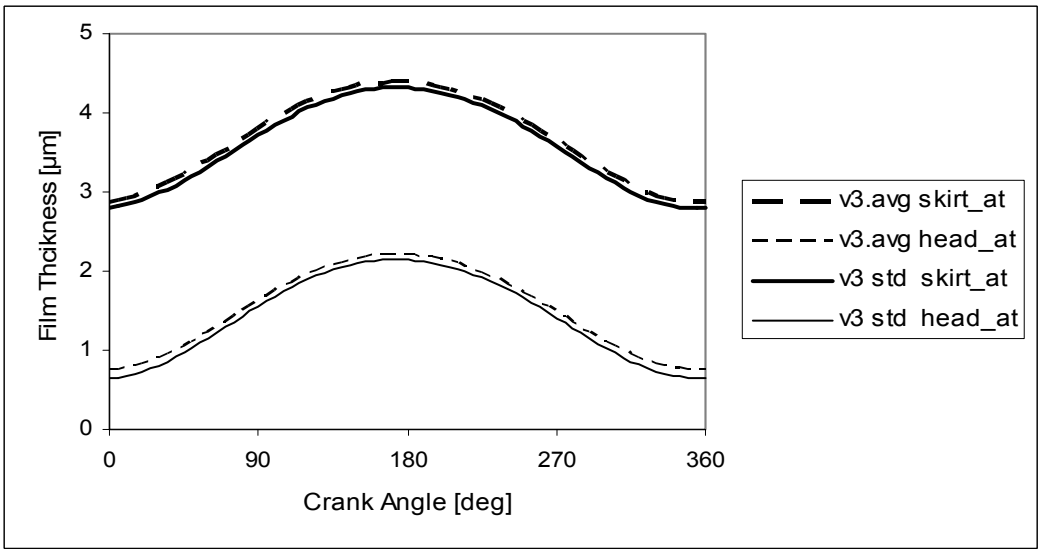

Figure A.2 Piston anti thrust side skirt and head film thicknesses of standard and average solutions for 0.003 Pa.s kinematic oil viscosit

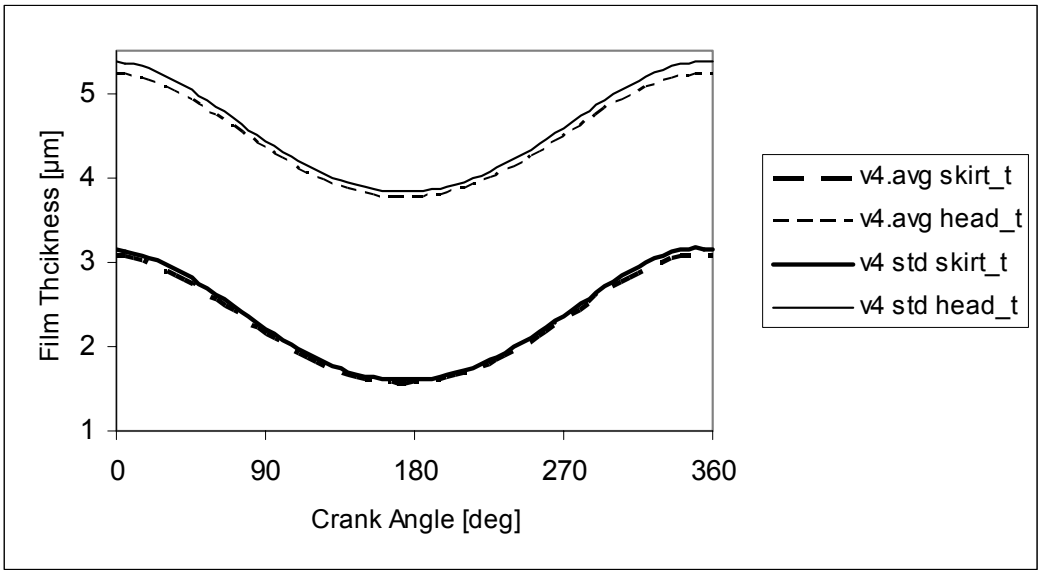

Figure A.3 Piston thrust side skirt and head film thicknesses of standard and average solutions for 0.004 Pa.s oil kinematic viscosity

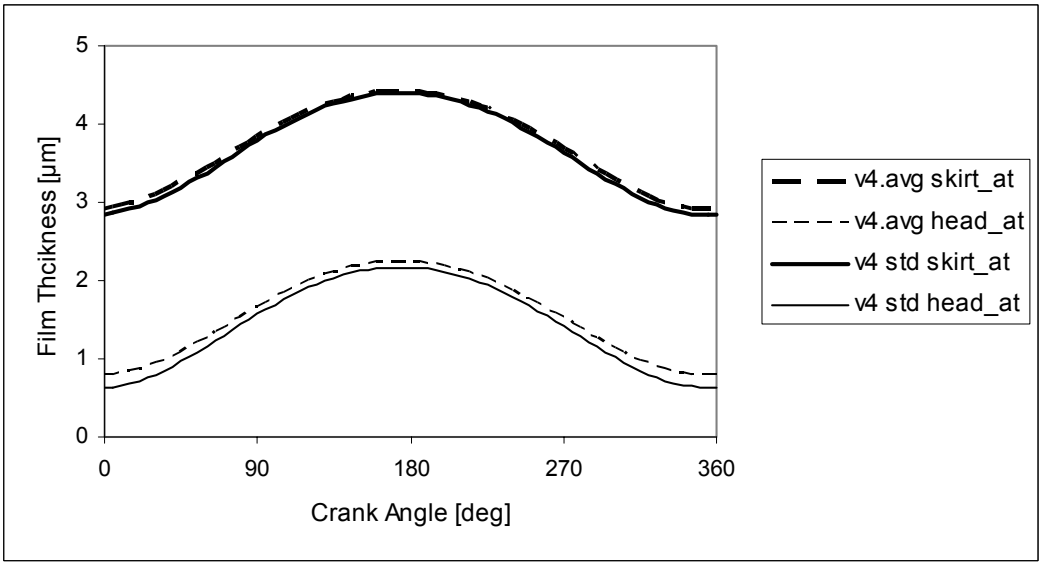

Figure A.4 Piston anti thrust side skirt and head film thicknesses of standard and average solutions for 0.004 Pa.s kinematic oil viscosity

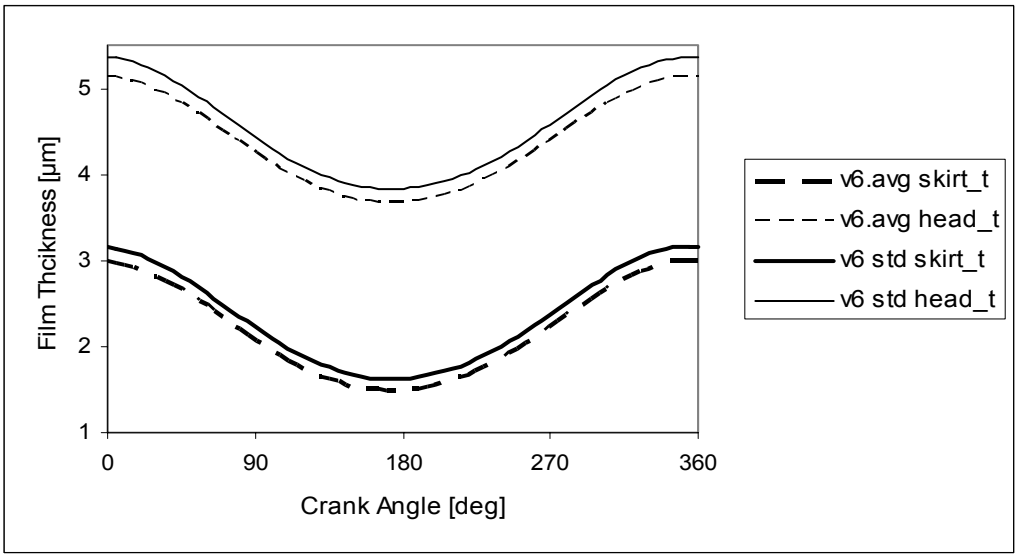

Figure A.5 Piston thrust side skirt and head film thicknesses of standard and average solutions for 0.006 Pa.s oil kinematic viscosity

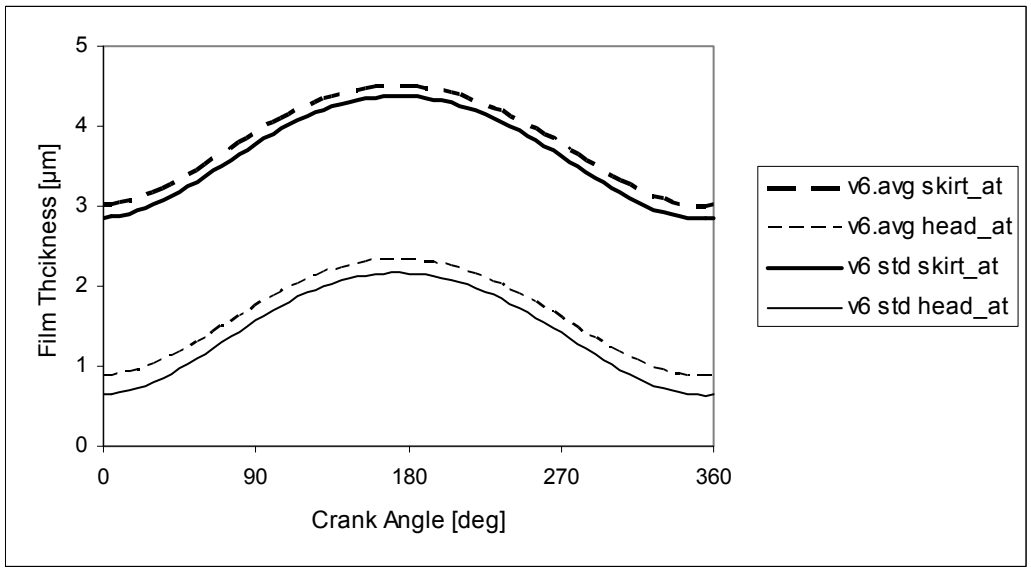

Figure A.6 Piston anti thrust side skirt and head film thicknesses of standard and average solutions for 0.006 Pa.s kinematic oil viscosity

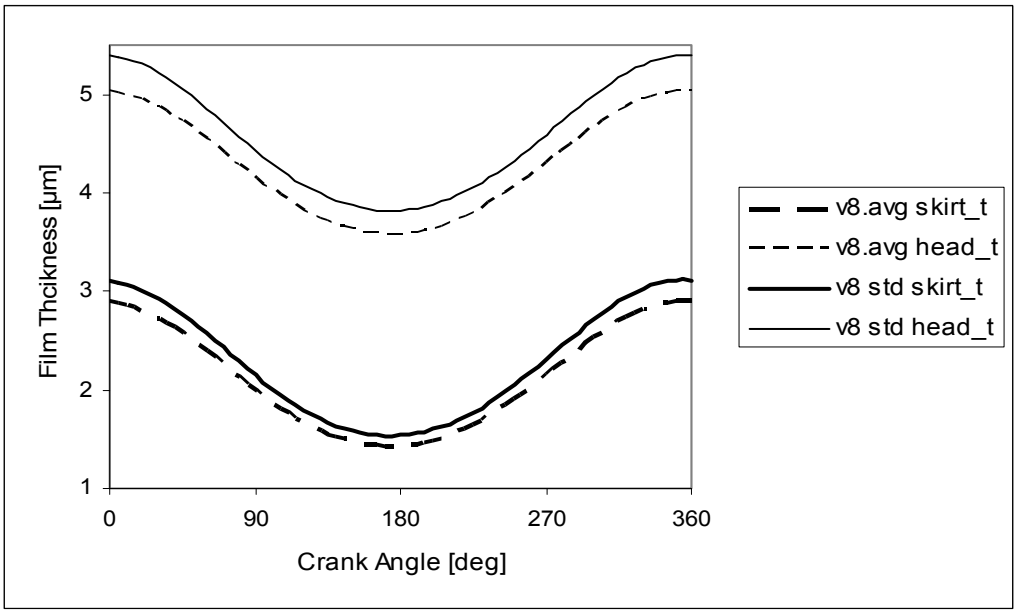

Figure A.7 Piston thrust side skirt and head film thicknesses of standard and average solutions for 0.008 Pa.s oil kinematic viscosity

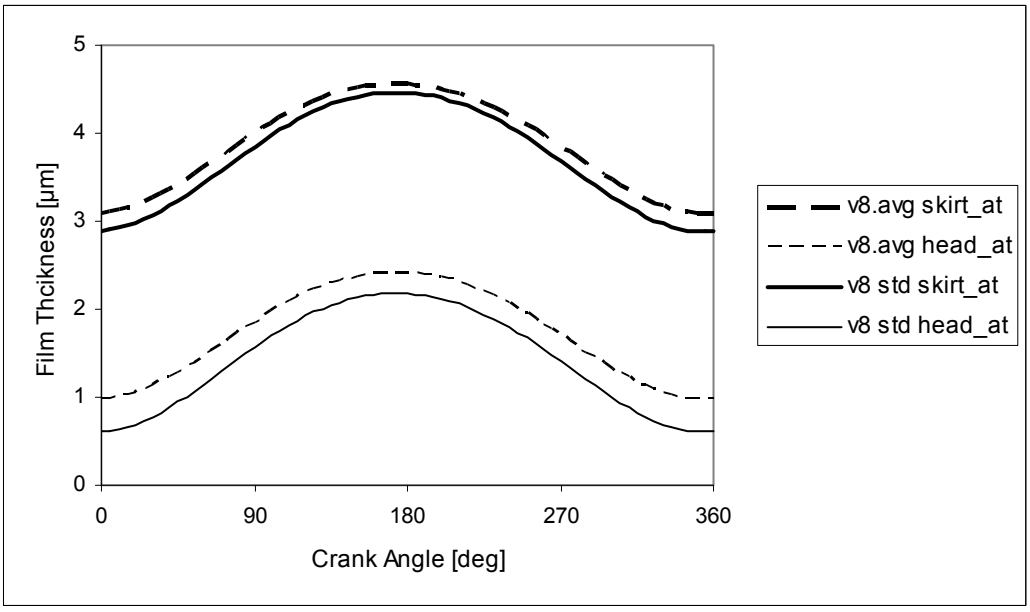

Figure A.8 Piston anti thrust side skirt and head film thicknesses of standard and average solutions for 0.008 Pa.s kinematic oil viscosity

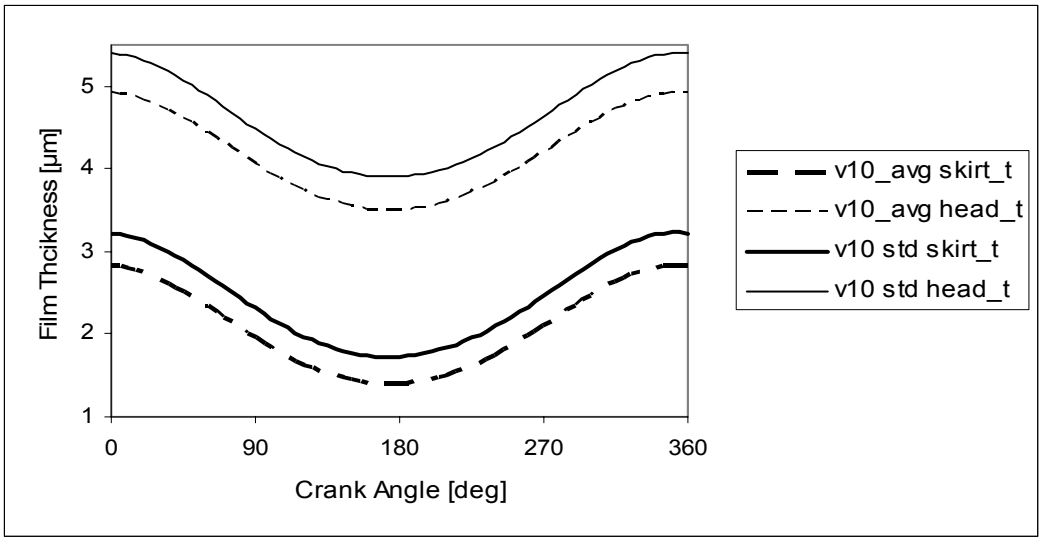

Figure A.9 Piston thrust side skirt and head film thicknesses of standard and average solutions for 0.010 Pa.s oil kinematic viscosity

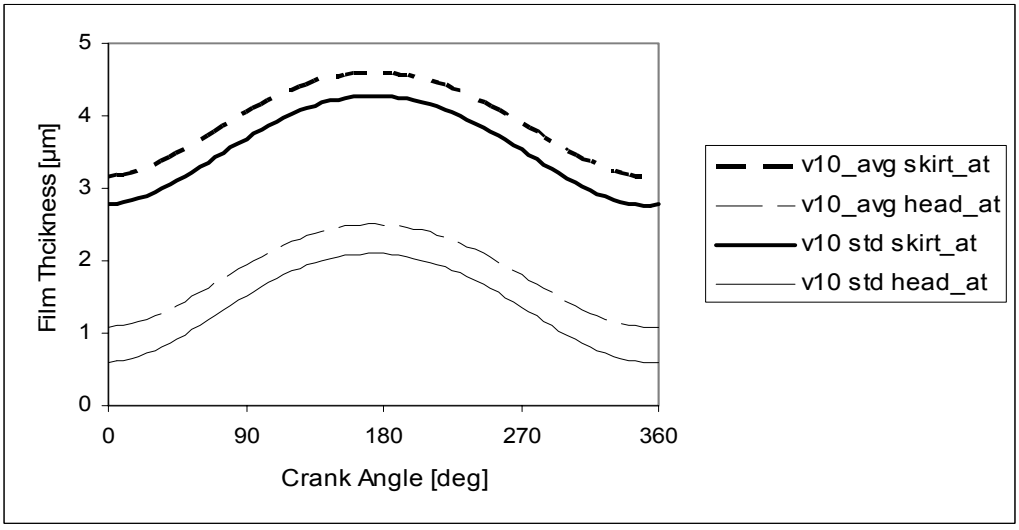

Figure A.10 Piston anti thrust side skirt and head film thicknesses of standard and average solutions for 0.010 Pa.s kinematic oil viscosity

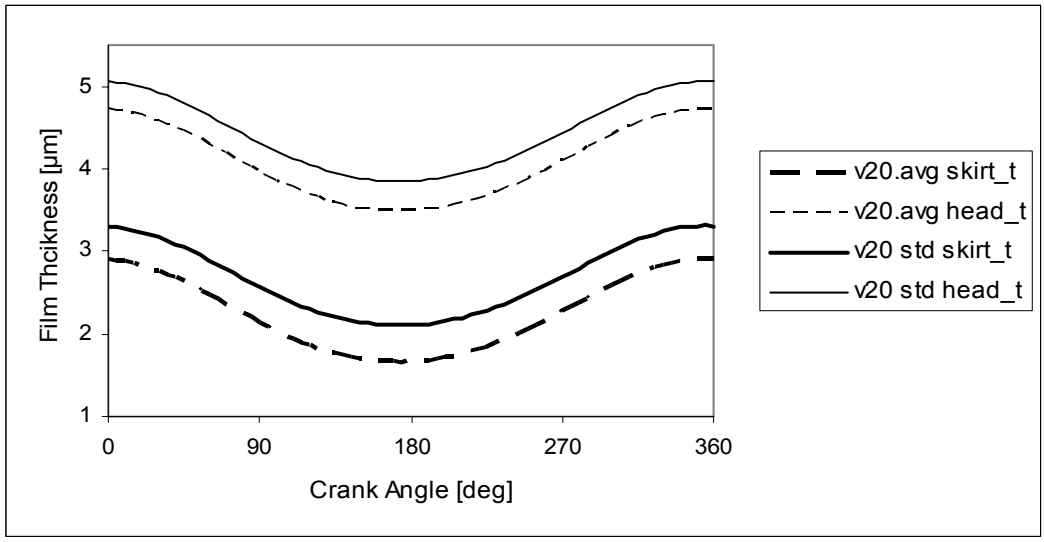

Figure A.11 Piston thrust side skirt and head film thicknesses of standard and average solutions for 0.020 Pa.s oil kinematic viscosity

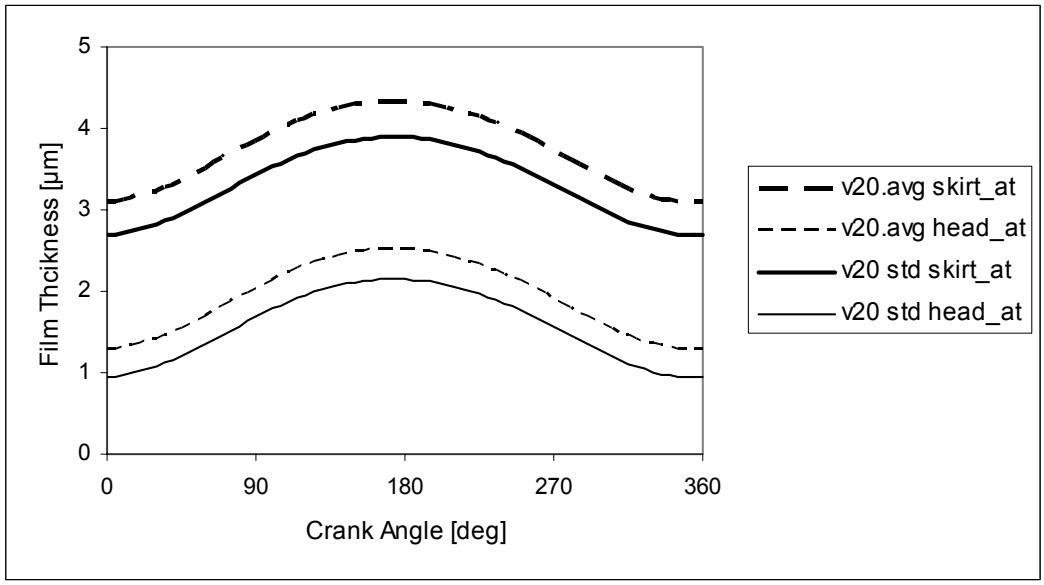

Figure A.12 Piston anti thrust side skirt and head film thicknesses of standard and average solutions for 0.020 Pa.s kinematic oil viscosity

REFERENCES

[1] Tower, B., 1883, “First Report on Friction Experiments”, Proc. Inst. Mech. Engrs., pp 632-659.

[2] Petrov, N. P., 1883, “Friction in Machines and the Effect of the Lubricant”, Inzh. Zh. St. Petersburg, Vol. 1, pp 71-140; Vol. 2 pp. 227-279; Vol. 3 pp.377-436; Vol. 4 pp. 535-564..

[3] Reynolds, O., 1886, “On the Theory of Lubrication and its Application to Mr. Beauchamp Tower’s Experiments Including an Experimental Determination of the Viscosity of Olive Oil”, Phil. Trans. Roy. Soc. London, Vol. 177, pp. 157-234.

[4] Hardy, W. B., and Doubleday, I., 1922, “Boundary Lubrication-The Paraffin Series”, Proc. Roy. Soc. London Ser. A. Vol. 100, Mar. 1, pp. 25-39.

[5] Hardy, W. B., and Doubleday, I., 1922, “Boundary Lubrication-The Temperature Coefficient”, Proc. Roy. Soc. London Ser. A. Vol. 101, Sept. 1, pp. 487-492.

[6] Bowden, F. P., Tabor, D., 2001 “The Friction and Lubrication of Solids”, Clarendon Press.

[7] Hamrock, B. J., 1994, Fundamentals of Fluid Film Lubrication, McGraw-Hill, Inc.

[8] Frene, J., Nicolas, D., Degueurce, B., Berthe, D. and Godet, M., 1997, Hydrodynamic Lubrication, Elsevier.

[9] Williams, J. A., 1994, Engineering Tribology, Oxford University Pres.

[10] Goenka, P. K., and Meernik, P. R., 1992**,** Lubrication Analysis of Piston Skirts, SAE Paper 920490

[11] Dursunkaya, Z., Keribar, K., 1992, “Simulation of Secondary Dynamics of Articulated and Conventional Piston Assemblies”, SAE Paper No. 920484.

[12] Keribar, K., Dursunkaya, Z., 1992, “A Comprehensive Model of Piston Skirt Lubrication”, SAE Paper No. 920483.

[13] Keribar, R., Dursunkaya, Z., and Ganapathy, V., 1993, “An Integrated Design Analysis Methodology to Adress Piston Tribological Issues”, SAE Paper No. 930793.

[14] Duyar, M. and Dursunkaya**,** Z., “Design Improvement of a Compressor Bearing Using an Elastohydrodynamic Lubrication Model,” International Compressor Engineering Conference at Purdue, July 16-19, West Lafayette Indiana, USA, 2002.

[15] Duyar, M. and Dursunkaya**,** Z., “Design Improvement Based on Wear of a Compressor Bearing Using an Elastohydrodynamic Lubrication Model,” International Compressor Engineering Conference at Purdue, July 17-20, 2006 West Lafayette Indiana, USA.

[16] Duyar, M., Elastohydrodynamic Lubircation Analysis and Design of a Journal Bearing, 2002, METU.

[17] Sommerfeld, A., 1904, “Zur Hydrodynamichen Theorie der Schiermittelreibung”, Z. angew. Math. Phys., 50, pp.97-155.

[18] Patir, N., Cheng, H.S., 1978, “ An Average Model for Determining Effects of Three-Dimensional Raughness on Partial Hydrodynamic Lubrication”, Transactions of the ASME Journal of Lubrication Technology, Vol.100, pp. 12-17.

[19] Patir, N., Cheng, H.S., 1979, “ Application of Average Flow Model to Lubrication Between Rough Sliding Surfaces”, Transactions of the ASME Journal of Lubrication Technology, Vol.101, pp. 220-230.

[20] McCool, J., I., 1988, “The Distrubution of Microcontact Area, Load, Pressure, and Flash Temperature Under the Greenwood-Williams Model”, ASME Journal of Tribology, Vol.110, pp.106-111

[21] Greenwood, I. A., and Tripp, J. H., 1971, “*The Contact of Two Nominally Flat Surfaces”*, Proc. IMechE., Vol. 185, pp. 625-633.

[22] Archard, J., F., 1953, “Contact of Rubbing Flat Surfaces”, Journal of Applied Physics, Vol. 24, pp.981-988

[23] Shigley, J. E. and Uicker, J. J., 1995, Theory of Machines and Mechanisms, McGraw-Hill, pp.605-632